AD-A154 218 COMPARISON OF 8 TO 12 MICROMETER AND 3 TO 5 MICROMETER CVF TRANSMISSOMETE..(U) AIR FORCE GEOPHYSICS LAB HANSCOM AFB MA F X KNEIZYS ET AL. 26 JUN 84 1/1

UNCLASSIFIED AFGL-TR-84-0171 F/G 20/6 NL

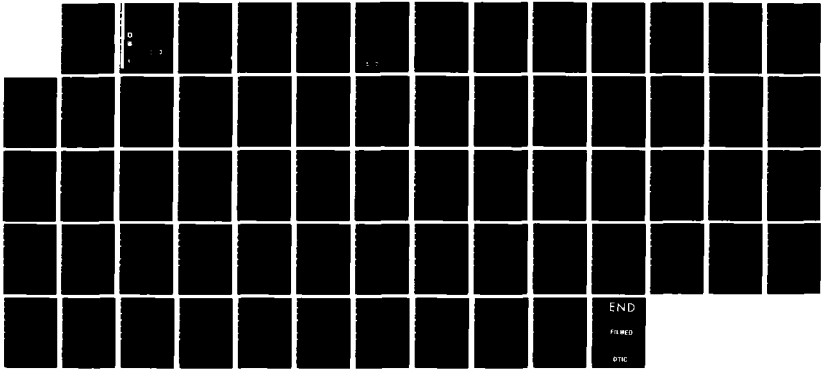

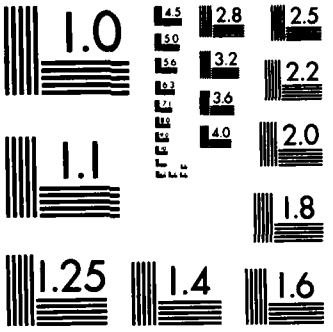

AFGL-TR-84-0171
ENVIRONMENTAL RESEARCH PAPERS, NO. 885

Comparison of 8 to 12 Micrometer and 3 to 5 Micrometer CVF Transmissometer Data With LOWTRAN Calculations

F. X. KNEIZYS
R. R. GRUENZEL
W. C. MARTIN
M. J. SCHUWERK
W. O. GALLERY
S. A. CLOUGH
J. H. CHETWYND, Jr
E. P. SHETTLE

26 June 1984

OPTICAL PHYSICS DIVISION
PROJECT 7670, 2004
AIR FORCE GEOPHYSICS LABORATORY
HANSCOM AFB, MA 01731

This report has been reviewed by the ESD Public Affairs Office (PA) and is releasable to the National Technical Information Service (NTIS)

"This technical report has been reviewed and is approved for publication"

FOR THE COMMANDER

BERTRAM D. SCHURIN, Chief
Infrared Physics Branch

JOHN S. GARING, Director
Optical Physics Division

Qualified requestors may obtain additional copies from the Defense Technical Information Center. All others should apply to the National Technical Information Service.

If your address has changed, or if you wish to be removed from the mailing list, or if the addressee is no longer employed by your organization, please notify AFGL/DAA, Hanscom AFB, MA 01731. This will assist us in maintaining a current mailing list.

Do not return copies of this report unless contractual obligations or notices on a specific document requi-es that it be returned.

AD-A154218

UNCLASSIFIED
SECURITY CLASSIFICATION OF THIS PAGE

REPORT DOCUMENTATION PAGE

1a. REPORT SECURITY CLASSIFICATION: Unclassified	1b. RESTRICTIVE MARKINGS
2a. SECURITY CLASSIFICATION AUTHORITY	3. DISTRIBUTION/AVAILABILITY OF REPORT: Approved for public release; distribution unlimited.
2b. DECLASSIFICATION/DOWNGRADING SCHEDULE	
4. PERFORMING ORGANIZATION REPORT NUMBER(S): AFGL-TR-84-0171 ERP No. 885	5. MONITORING ORGANIZATION REPORT NUMBER(S)
6a. NAME OF PERFORMING ORGANIZATION: Air Force Geophysics Laboratory; 6b. OFFICE SYMBOL (If applicable): OPI	7a. NAME OF MONITORING ORGANIZATION
6c. ADDRESS (City, State and ZIP Code): Hanscom AFB, Massachusetts 01731	7b. ADDRESS (City, State and ZIP Code)
8a. NAME OF FUNDING/SPONSORING ORGANIZATION; 8b. OFFICE SYMBOL (If applicable)	9. PROCUREMENT INSTRUMENT IDENTIFICATION NUMBER
8c. ADDRESS (City, State and ZIP Code)	10. SOURCE OF FUNDING NOS

PROGRAM ELEMENT NO	PROJECT NO.	TASK NO	WORK UNIT NO
62101F 62204F	7670 2004	7670 09 2004 05	7670 09 07 2004 05 53

11. TITLE (Include Security Classification): (see reverse)

12. PERSONAL AUTHOR(S): F.X. Kneizys, R.R. Gruenzel*, W.C. Martin*, M.J. Schuwerk*, W.O. Gallery**, S.A. Clough, J.H. Chetwynd, Jr., E.P. Shettle

13a. TYPE OF REPORT	13b TIME COVERED	14. DATE OF REPORT (Yr., Mo., Day)	15. PAGE COUNT
Scientific, Interim.	FROM _____ TO _____	1984 June 26	62

16. SUPPLEMENTARY NOTATION
*Air Force Wright Aeronautical Laboratories
**Present address OptiMetrics, Inc.

17 COSATI CODES		
FIELD	GROUP	SUB GR
04	01	

18. SUBJECT TERMS (Continue on reverse if necessary and identify by block number)
Atmospheric Transmittance; Attenuation; Atmospheric Optics; Absorption; Infrared; Aerosols

19. ABSTRACT (Continue on reverse if necessary and identify by block number)

This report contains a description and analysis of a series of atmospheric transmittance measurements taken at the Targeting Systems Characterization Facility, Wright-Patterson Air Force Base, Ohio with a circular variable filter (CVF) transmissometer. The data cover the spectral regions from 8- to 12-μm and from 3- to 5-μm for both 8-km and 2.25-km atmospheric paths. The instrumentation is described and comparisons of the data with calculations using the atmospheric transmittance and background radiance code, LOWTRAN 6, are presented.

20. DISTRIBUTION/AVAILABILITY OF ABSTRACT	21. ABSTRACT SECURITY CLASSIFICATION
UNCLASSIFIED/UNLIMITED ☐ SAME AS RPT ☒ DTIC USERS ☐	Unclassified

22a. NAME OF RESPONSIBLE INDIVIDUAL	22b. TELEPHONE NUMBER (Include Area Code)	22c. OFFICE SYMBOL
Francis X. Kneizys	(617)861-3654	AFGL/OPI

DD FORM 1473, 83 APR EDITION OF 1 JAN 73 IS OBSOLETE

UNCLASSIFIED
SECURITY CLASSIFICATION OF THIS PAGE

11. Title

Comparison of 8 to 12 Micrometer and 3 to 5 Micrometer CVF Transmissometer Data With LOWTRAN Calculations

Contents

Illustrations

Illustrations

Tables

Comparison of 8 to 12 Micrometer and 3 to 5 Micrometer CVF Transmissometer Data With LOWTRAN Calculations

1. INTRODUCTION

This report represents a joint effort by the Air Force Wright Aeronautical Laboratories (AFWAL), Wright-Patterson AFB, Ohio, and the Air Force Geophysics Laboratory (AFGL), Hanscom AFB, Mass., to present and analyze a series of atmospheric transmittance measurements taken in the summer of 1981. The data consists of preliminary atmospheric transmittance measurements in the 8- to 12-μm and the 3- to 5-μm regions taken at Wright-Patterson AFB over both an 8-km and a 2.25-km path. A Memorandum of Agreement existed between the two laboratories to exchange measurements and models of atmosphere effects on optical sensors. As part of this agreement, these measurements were compared with the latest low-resolution atmospheric transmittance model, LOWTRAN 6.[1] Section 2 of this report describes the facilities and measurements observed, and Section 3 contains the analysis of the data.

It should be emphasized at the beginning that these measurements were a preliminary effort designed mainly to test the system. Many of the system components, (for example, visible transmissometer, particle size counters, and

(Received for publication 26 June 1984)

1. Kneizys, F.X., Shettle, E.P., Gallery, W.O., Chetwynd, Jr., J.H., Abreu, L.W., Selby, J.E.A., Clough, S.A., and Fenn, R.W. (1983) Atmospheric Transmittance/Radiance: Computer Code LOWTRAN 6, AFGL-TR-83-0187, AD A137786.

meteorological sensors) were not operational at the time. Therefore, the conclusions based on the data are tentative. Future measurements with all sensors operational are planned that will provide transmittance measurements with a much more accurate characterization of the atmosphere. However, we feel that these preliminary measurements are significant enough to be of interest to the scientific community and to electro-optical system designers.

2. DESCRIPTION OF THE FACILITIES AND THE MEASUREMENTS

2.1 Introduction

The Targeting Systems Characterization Facility (TSCF) has been established at AFWAL/AARI, Wright-Patterson AFB, Ohio to meet the Air Force needs for improved methods to predict weather and associated environmental effects that could impact the employment of tactical electro-optical systems. Of particular concern are those systems that use TV, infrared, and millimeter wave sensors.

There are three major components of the TSCF: the sensor platform, the target complexes, and an array of meteorological instruments along the optical path from the sensor platform to the target area. The facility was designed to quantitatively relate the performance of targeting systems with the natural environment in which they will be required to operate.

The sensor platform is located in the upper floors and atop the Wright-Patterson AFB, Area B, Building 620, Twin Towers. This platform can house sensors in various stages of development. permits side-by-side comparisons, and provides several operator positions for human factors experimentation.

Located 8-km east of Building 620 is the Trebein Reservation. Also, 2.25-km west of Building 620, a mobile targeting complex has been established to support this effort. At both complexes, a variety of manmade targets including a large area target, mobile thermal target, impulse function targets (visual, near infrared, and infrared), bar targets. and military vehicles can be deployed.

Instrumentation gathers meteorological data atop Building 620, atop a 130 ft tower at the mid-point between Building 620 and Trebein, and at Trebein. Measurements include temperature, dewpoint, windspeed and direction, barometric pressure, rainfall amount, particle size distribution, forward and integrated scatter, and all-sky radiation. A mobile meteorological facility can also be used to support sensor evaluation experimentation over paths other than the fixed 8-km path. The meteorological instrumentation duplicates that found at the three fixed sites and is primarily used to support efforts at the 2.25-km complex.

Transmission in the infrared, for narrow wavelength bands, can also be measured over either the 8- or 2.25-km paths. The transmissometer source is located atop Building 620 and the receiver can be positioned at either the 8- or 2.25-km target complex.

Signal processing and recording of the meteorological data begins with the microprocessor at each instrument site including the mobile data pole. The microprocessor allows variable sampling rates and various sampling techniques. It samples and digitizes the output from the instruments. The information is sent via telephone or direct line to Building 622, Area B, for recording and storage. Building 622 houses the computer support function, where data collection, processing, and storage is accomplished utilizing HP 2112A and HP 2113A minicomputer systems. The computer capability also supports the atmospheric effects measurement program and laboratory sensor evaluation, providing real-time analog-to-digital conversion of video data with on-line computation of performance parameters. A dedicated HP 2117A minicomputer is interfaced to the central computer net for expanded computation and storage capability. The transmissometer data is recorded on a strip chart recorder. The data is then entered into a computer data base using programs developed for this purpose and for comparison of the transmissometer data on a day-to-day basis using LOWTRAN[1,2] predictions. Concurrent meteorological data are used as input.

2.2 Transmissometer Design

Because of problems encountered with commercial transmissometers, the Air Force Avionics Laboratory embarked upon an effort to design and build a multiband transmissometer unit that eliminated the problems encountered with these commercial units.

The optical schematic of the receiver unit is shown in Figure 1. An off-axis parabolic mirror with an 8 in. unobstructed diameter and 25 in. focal length is used to collect the collimated source energy. The energy is spectrally split by two dichroic beamsplitters. The first dichroic reflects the visible radiation and transmits the infrared radiation; the second reflects the 3- to 5-μm radiation and transmits the 8- to 14-μm radiation. Each channel has an appropriate circular variable filter (CVF) immediately in front of its detector. The detectors are Si, InSb, and HgCdTe for the visible, 3- to 5-μm and 8- to 14-μm channels of the transmissometer. Each dichroic beamsplitter has a minimum transmission

---

2. Kneizys, F.X., Shettle, E.P., Gallery, W.O., Chetwynd, Jr., J.H., Abreu, L.W., Selby, J.E.A., Fenn, R.W., and McClatchey, R.A. (1980) Atmospheric Transmittance/Radiance: Computer Code LOWTRAN 5, AFGL-TR-80-0067, AD A088215.

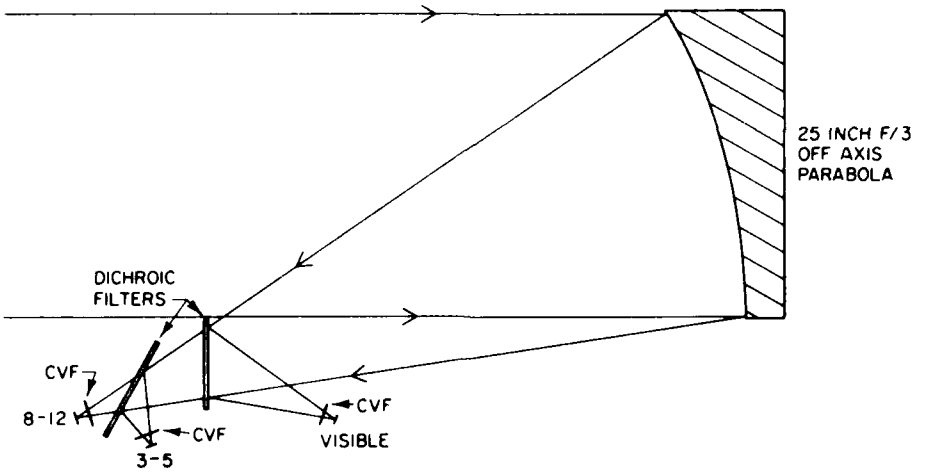

Figure 1. Optical Schematic of Transmissometer Receiver

and/or reflection value, as the case may be, in excess of 80 percent. They are multilayer coatings made by Optical Coating Laboratories, Inc., specifically for this application. The 3- to 5-μm CVF has a 2 percent wavelength half-bandwidth, and the 8- to 14-μm CVF has a 6 percent wavelength half-bandwidth. However, because a finite area of each CVF is illuminated, an additional 0.025-μm bandwidth is present for the 3- to 5-μm channel, and an additional 0.27-μm bandwidth is present in the 8- to 14-μm channel. This translates to a 50- to 90-wavenumber half-bandwidth for the 3- to 5-μm data and 60- to 115-wavenumber half-bandwidth for the 8- to 14-μm data.

The visible blur circle of the parabolic mirror is very nearly diffraction limited in size (less than 0.05 mm in diameter) at best focus. This is an order of magnitude smaller than the smallest detector in the system. Therefore, the spot image should remain on the detectors if turbulence induced beam wander occurs during measurement.

What is accomplished with this new receiver design is a threefold increase in the amount of energy collected, and improved accuracy due to the small spot size and consequent flat field-of-view. Since the energy is focused down to a small spot on the detectors, the accuracy of measurement depends on the responsivity-uniformity of each detector surface. In the case of Si and InSb, there was no problem. Each detector was measured and found to be uniform to at least ± 2 percent. And, because of the unobstructed nature of the receiver optics, it is

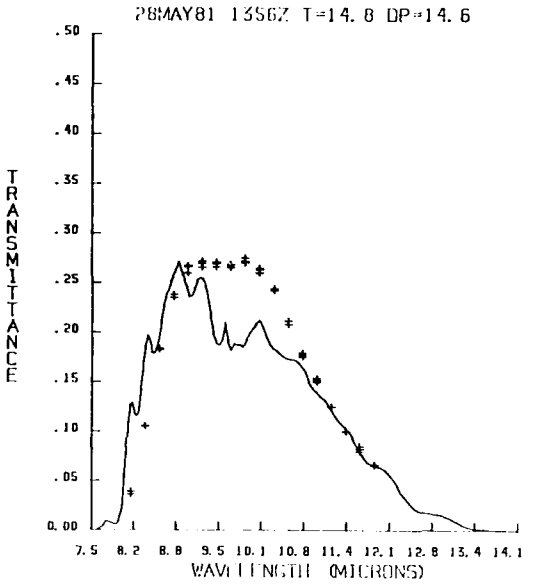

Figure 11. Sample Transmittance Measurements (+) and Calculated LOWTRAN 5 Transmittance Without Aerosols (—) Under Conditions of High Humidity and Low Visibility, 8- to 14-μm Region (28 May 81, 1356Z, 8-km Path)

LOWTRAN 6, and in particular, the new water vapor continuum model. The results of that analysis are presented here.

The data consists of the CVF transmissometer data in the 3- to 5-μm and 8- to 12-μm ranges for both the 8-km and 2.25-km paths. Examples of these measurements are shown in Figures 9 and 10. In addition, simultaneous measurements of temperature and dewpoint were taken at the top of Building 620. No detailed measurements of aerosol properties are available. However, there are observer estimates of meteorological range. A complete list of the CVF transmissometer data, temperature, dewpoint measurements, and the estimated value of the meteorological range (VIS), are included in Appendix A. The observer's comments are included as Appendix B.

3.2 Method of Analysis

The goal of this analysis is to validate the LOWTRAN[1,2] transmittance model in the 3- to 12-μm and 3- to 5-μm windows. In these spectral regions, the transmittance is primarily determined by absorption of the water vapor continuum and

channel appeared to have the same signal level stability obtainable with the 3- to 5-μm channel. However, because of the numerous adjustments implemented during the final stages of laboratory checkout and calibration, another goal of this test series was to determine the long-term stability of the 8- to 14-μm detector electronics. Therefore, although the meteorological support was not optimum for a detailed model verification effort, the measurement program was undertaken to quantify some of the performance parameters of the transmissometer.

The initial measurements were recorded under good visibility and low absolute humidity conditions. Although the 8- to 14-μm signals were significantly lower in signal-to-noise ratio than the 3- to 5-μm signals, it was possible to record the output voltage of the lock-in-amplifier and reliably repeat these measurements under stable meteorological conditions. The 3- to 5-μm and 8- to 14-μm measurments were then compared with LOWTRAN 5 predictions, using the available meteorological data. The measured values of transmission under these conditions compared reasonably well with the model predictions, such as the examples shown in Figures 9 and 10. However, somewhat later in the test period, measurements were recorded on days that visibility was observer estimated as poor to fair, and the relative and absolute humidity was high. When these measurements were compared to LOWTRAN 5 predictions, it was observed that the measured 8- to 14-μm transmission significantly exceeded the predicted model predictions even when aerosol extinction was excluded as model inputs. Examples of some of these measurements over the 8-km path are shown in Figures 11 and 12.

Since these computer model-to-measurements comparisons are dependent on the accuracy of the transmissometer measurement and on the accuracy of the TSCF meteorological instrumentation, an effort was undertaken during this measurement period to qualify the temperature-dewpoint recordings. This investigation showed that the temperature-dewpoint outputs contained ± 0.75 degrees C of noise.

3. ANALYSIS OF THE DATA

3.1 Introduction

As part of the Memorandum of Agreement between AFWAL/AARI and AFGL/OPI, "Atmospheric Effects Measurement and Modeling", AFWAL supplied AFGL with the preliminary transmissometer data taken between 7 May and 17 August 1931 for analysis. AFGL/OPI and OPA have analyzed this data with the goal of validating the latest version of the atmospheric transmittance/radiance model,

Table 3. Transmittance Values Over the 8-km Path at Selected Filter Positions, With and Without Broadband Filters

Wavelength	Measured Without Filter	Measured With Black Filter	Measured With Aluminum Filter	Calculated Black Filter	Calculated Aluminum Filter
8.74-μm	0.655	0.070	0.063	0.082	0.069
9.62-μm	0.670	0.077	0.067	0.084	0.069
10.62-μm	0.735	0.082	0.070	0.087	0.074

to the nearness of this wavelength to the edge of an atmospheric transmission band, and therefore susceptible to larger calibration and measurement errors.

2.5 Measurements

The 3- to 5-μm and 8- to 14-μm channels of the transmissometer were calibrated on 5 May 1981, and the receiver unit was installed at the 8-km Trebein site. Narrow band transmission measurements were recorded periodically between 7 May and 24 June 1981. The unit was recalibrated on 30 June 1981 and then installed at the 2.25-km site. A series of measurements were recorded periodically between 22 July and 17 August 1981. During these data collection periods, the meteorological stations of the TSCF were being modified in order to initiate operation of meteorological support at the 2.25-km site. To accomplish this goal, it was necessary to terminate operation of the 4-km and Trebein meteorological stations. Therefore, during the 8-km test period, only the meteorological station at the transmissometer source site was operational. Occasional support was supplied by the 2.25-km station, which is in the opposite direction from the 8-km path. Also, the forward scatter meters were removed from the TSCF for recalibration; and, therefore, the visibility had to be observer estimated.

The intent of this test series, however, was to determine the feasibility of reliably obtaining 8- to 14-μm narrow band transmission measurements over an 8-km path. Although reliable 3- to 5-μm narrow band transmission measurements had been successfully obtained over this distance, the 100 to 1 difference in the preamp outputs between the 3- to 5-μm and 8- to 14-μm channels resulted in signals for the 8- to 14-μm channel which were significantly lower in signal-to-noise ratio. It was questionable whether there would be enough signal to use the lock-in-amplifier electronics at this range. Except for the inherent 3 percent drop in signal level noted during the laboratory evaluation, the 8- to 14-μm

Table 2. Transmittance Values in the Lab at Selected Filter Positions With and Without Broadband Filters

No Filter		Black Filter		Aluminum Filter	
Pinhole Diameter	Preamp Voltage	Preamp Voltage	Transmission %	Preamp Voltage	Transmission %
CVF Filter Position #23 (8.74-μm)					
0.0256 in.	93.0 mv	11.6 mv	12.5%	9.86 mv	10.6%
0.0140 in.	27.4 mv	3.46 mv	12.6%	2.93 mv	10.7%
0.0081 in.	9.00 mv	1.14 mv	12.7%	0.962 mv	10.7%
0.0048 in.	2.86 mv	0.362 mv	12.7%	0.306 mv	10.7%
CVF Filter Position #39 (9.62-μm)					
0.0256 in.	85.6 mv	10.8 mv	12.6%	9.12 mv	10.7%
0.0140 in.	25.2 mv	3.19 mv	12.7%	2.71 mv	10.8%
0.0081 in.	8.24 mv	1.05 mv	12.7%	0.886 mv	10.8%
0.0048 in.	2.61 mv	0.332 mv	12.7%	0.281 mv	10.8%
CVF Filter Position #57 (10.62-μm)					
0.0256 in.	75.8 mv	8.96 mv	11.8%	7.58 mv	10.0%
0.0140 in.	22.3 mv	2.66 mv	11.9%	2.25 mv	10.1%
0.0081 in.	7.27 mv	0.871 mv	12.0%	0.736 mv	10.1%
0.0048 in.	2.29 mv	0.276 mv	12.1%	0.232 mv	10.1%

filters were then used in a field experiment to quantify the measurement accuracy of τ over the 8-km range. The transmissometer receiver was set up at the Trebein site and the transmission was measured at the same CVF positions that were calibrated in the laboratory. Each filter was then inserted into the collimator source optics, and the transmission of the combined effect, broadband filter plus atmospheric transmission, was measured. These results are shown in Table 3. Comparing these measured values with the values we should have measured show a maximum error of 6 percent of τ at 10.62 μm, 9 percent of τ at 9.62 μm, and 16 percent of τ at 8.74 μm. The largest errors were obtained when using the black filter and could possibly be explained by a nonuniformity over the filter surface. In the laboratory calibration of these filters, much more of the surface area of the filter is "seen" by the detector than during field measurements. The larger error for both filters at the 8.74-μm position is probably attributable

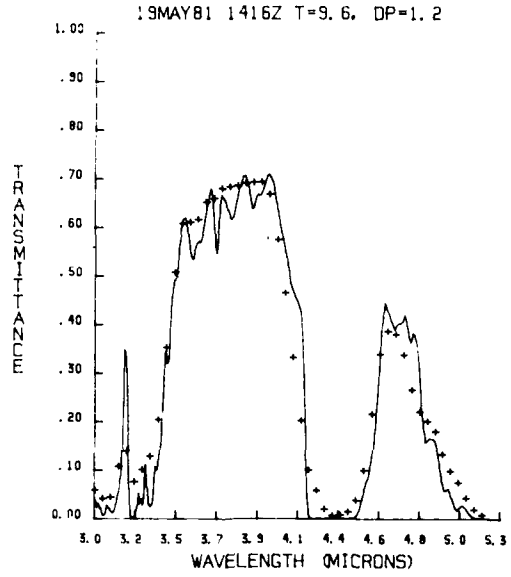

Figure 9. Sample Transmittance Measurement (+) and LOWTRAN 5 Calculation (—) vs Wavelength in the 3- to 5-μm Region (19 May 81, 1416Z, 8-km Path)

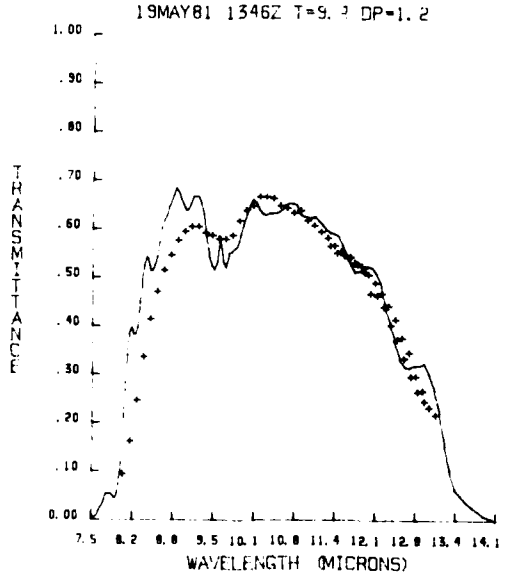

Figure 10. Sample Transmittance Measurement (+) and LOWTRAN 5 Calculation (—) vs Wavelength in the 3- to 5-μm Region (19 May 81, 1346Z, 8-km Path)

Table 1. Example of the Preamp and Postamp Outputs of a Calibration

d_s (in.)	$\frac{\pi d_s^2}{4}$ (cm^2)	Preamp Output (mv)	Postamp* Output (V_c) (mv)	$V_c / \pi d_s^2/4$
9.7-μm Position of 8 to 12 CVF				
0.0256	3.339×10^{-3}	315.2	1431.0	4.286×10^5
0.0140	1.003×10^{-3}	93.8	417.5	4.16×10^5
0.0081	3.300×10^{-4}	30.9	138.4	4.19×10^5
0.0048	1.167×10^{-4}	9.76	44.85	3.84×10^5
0.0046	1.072×10^{-4}	9.76	44.85	4.18×10^5
4.6-μm Position of 3 to 5 CVF				
0.0256	3.339×10^{-3}			
0.0140	1.003×10^{-3}	12875		
0.0081	3.300×10^{-4}	4331	433.0	1.31×10^6
0.0048	1.167×10^{-4}	1403	140.2	1.20×10^6
0.0046	1.072×10^{-4}	1403	140.2	1.31×10^6

*Postamp Output Attenuated by a Factor of 37.9

During discussions between AFWAL/AARI and AFGL/OP concerning the verification of linearity, and therefore quantitatively determining the measurement accuracy of low transmissions obtained over an 8-km range, it was suggested by AFGL/OP that the problem could possibly be solved utilizing a neutral density or broadband filter of known transmittance. Two such filters existed at AFGL/OP and were loaned to AFWAL/AARI. A series of measurements were made using each pinhole without the broadband filter. Then, the filters were inserted into the collimator source optics between the primary mirror and the aperture wheel pinholes. Measurements were made at three CVF positions corresponding to wavelengths centered at 8.74, 9.62, and 10.62-μm. The transmission values for these broadband filters using different pinholes of the collimator source are shown in Table 2. The results are in excellent agreement and demonstrate that the detector-electronics are linear over a dynamic range, equivalent to the range encountered between calibration and the measurement of low transmissions over an 8-km range. These

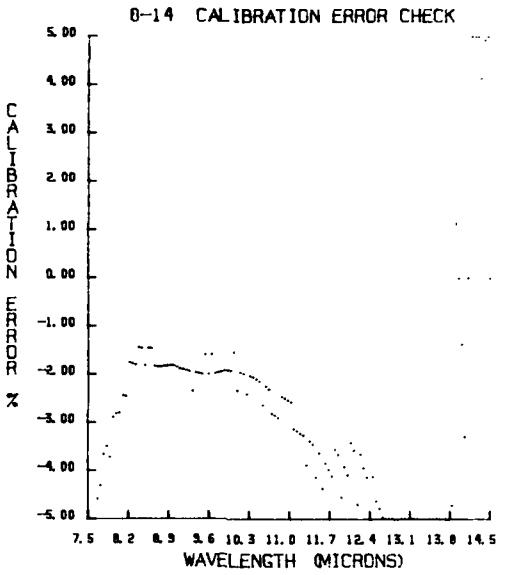

Figure 8. Comparison of Two Calibration Runs Taken 45 Days Apart, 8- to 14-μm Region

Several schemes were devised in an attempt to verify the linearity of the detector electronics over the dynamic range of voltages between calibration and the measurement of τ over an 8-km range. Measurements were made using the smaller pinholes that are part of the collimator aperture wheel, but the results obtained were always significantly less than the calibration values obtained with the larger pinholes. However, these smaller pinholes, which are 64 and 121 μm in diameter, approach the wavelength of IR radiation. When this occurs, the geometric optics approach to the calibration scheme is no longer valid since a significant amount of energy irradiating these small apertures is diffracted out of the f/3 cone of the collimator source optics. An attempt was also made to check linearity using a combination of large aperture wheel pinholes, and then stopping down the receiver optics using a series of smaller calibrated apertures. However, since the 8- to 14-μm detector assembly contains a field lens that images the receiver optics pupil onto the nonuniform HgCdTe detector, a change in the receiver optics pupil size results in an unpredictable change in the detector output. The demagnified image on the detector illuminates a smaller area of the detector chip; and because of the detector's nonuniform responsivity, the outputs are not proportional to the receiver pupil sizes.

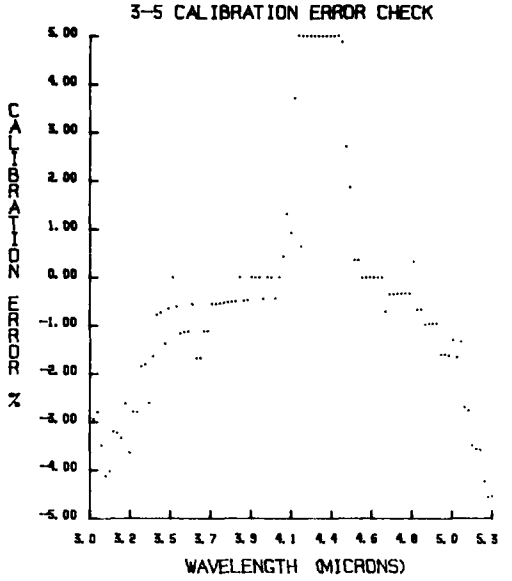

Figure 6. Comparison of Two Calibration Runs Taken 45 Days Apart, 3- to 5-μm Region

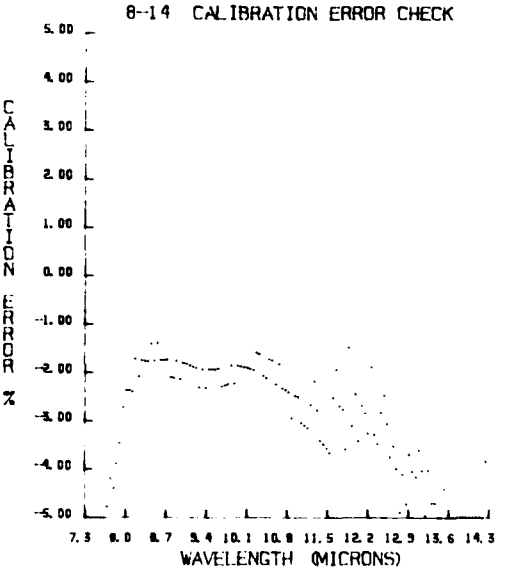

Figure 7. Comparison of Two Calibration Runs Taken 45 Days Apart, 8- to 14-μm Region

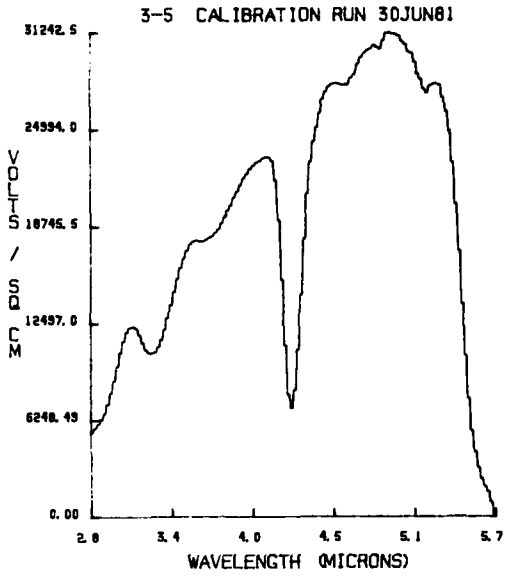

Figure 4. Sample of Transmissometer Calibration Run, 3- to 5-μm

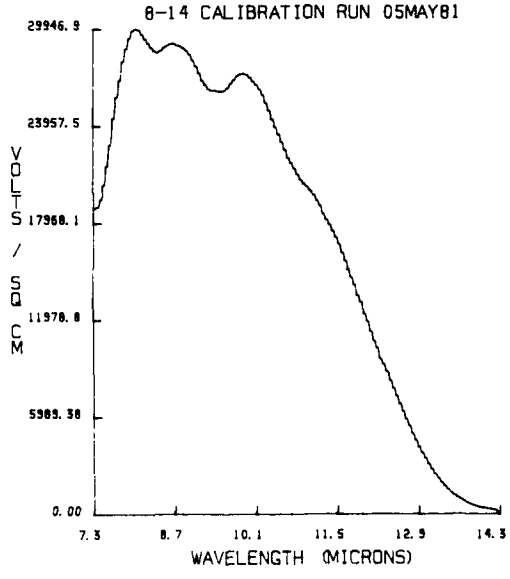

Figure 5. Sample of Transmissometer Calibration Run, 8- to 14-μm

measurement of transmission because the InSb detector response is uniform. However, because of the field lens in the HgCdTe detector assembly used for 8- to 14-μm transmission measurements, the limiting aperture inserted for calibration must remain in place during the measurement of transmission. Since 3- to 5-μm and 8- to 14-μm measurements are usually made simultaneously, this limiting aperture is now a permanent part of the receiver optics and $A_r = A_e$ in Eq. (6). Therefore,

$$\tau = \frac{\pi d_s^2 R^2 V_r}{4 f^2 A_c V_c} \quad . \tag{7}$$

To calibrate, a series of readings at each CVF position are recorded using several different pinhole apertures of diameter, d_s, at the focus of the source collimator. The properly normalized voltage readings, $V_c / d_s^2/4$, are averaged, and correspond to values that are proportional to the radiant intensity of the collimator source at that CVF position. An example of the 3- to 5-μm and 8- to 14-μm calibrations are shown in Figures 4 and 5. A comparison of two calibrations taken 45 days apart are shown in Figures 6, 7, and 8. Figures 7 and 8 are calibration comparisons for two different CVF filters. The calibrations are repeatable to a precision of ± 1 percent within the major IR transmission bands in the atmosphere. The error increases significantly at the edges of the transmission bands, and may be attributed to changes in the laboratory environment during each calibration and slight differences in the seating position of the CVF filter from run to run.

An example of the preamp and postamp outputs of a calibration are shown in Table 1. The calibration constant, $V_c / d_s^2/4$, for the larger diameter collimator aperture pinholes (0.0256, 0.0140, and 0.0081 in.), gives consistent values within the ability to measure the aperture diameters. The value obtained for the smallest aperture, 0.0048 in., departs from the average value of the larger apertures by 10 percent. However, if the value of this aperture is assumed to be 0.0046 in., the values now obtained for both the 4.6- and 9.7-μm calibrations are consistent with the values obtained for the larger apertures. Therefore, only those apertures 0.0081 in. or larger are used to calculate an average calibration value at each CVF position. It is assumed that the detector, preamp, and postamp electronics are linear over the entire range of measurable voltages. This assumption appears valid since measurements made over the 8-km path during periods of low to moderate absolute humidity, and moderate to high visibility, result in values of τ that compare favorably to LOWTRAN model predictions; using the prevailing meteorological data as input. An example of such comparisons are shown in Figures 9 and 10.

$$\frac{\frac{V_c}{A_e} A_c}{\frac{\pi d_s^2}{4 f^2}} \alpha I \quad . \tag{3}$$

The solid angle subtended by the receiver at range R when making transmission measurements is

$$\Omega = \frac{A_r}{R^2} \quad , \tag{4}$$

where A_r is the area of the receiver aperture in cm^2. V_r, the voltage reading during measurement, is proportional to the total power, Φ, collected by the receiver,

$$V_r \alpha \Phi \quad . \tag{5}$$

Since the same detector is used for calibration and measurement, and if the detector electronics are linear, then proportionality becomes equality when Eqs. (3), (4), and (5) are substituted into Eq. (1). Thus the transmission is

$$\tau = \left(\frac{\frac{V_c}{A_e} A_c}{\frac{\pi d_s^2}{4 f^2}} \right)^{-1} \frac{\frac{V_r}{A_r}}{\frac{R^2}{}} \quad . \tag{6}$$

The focal length of the collimator, f, the diameters of the pinhole apertures placed at the focus of the collimators, d_s, and the areas of apertures A_e, A_c, and A_r are measured in the laboratory. The most sensitive and difficult measurements are those that determine d_s. An error of 0.00025 cm in the measurement of even the largest diameter pinholes used in the calibration scheme can result in a 1 to 2 percent error in the calibration value.

Because the 8-in. receiver aperture diameter is smaller than the 16-in. source collimator aperture diameter, and the secondary mirror of the source collimator causes a central obscuration of the transmitted radiation during calibration, it is necessary to insert a smaller aperture, A_e, in front of the receiver aperture, A_r, during calibration. If only 3- to 5-μm transmission measurements were made, it would be possible to remove this limiting aperture during the

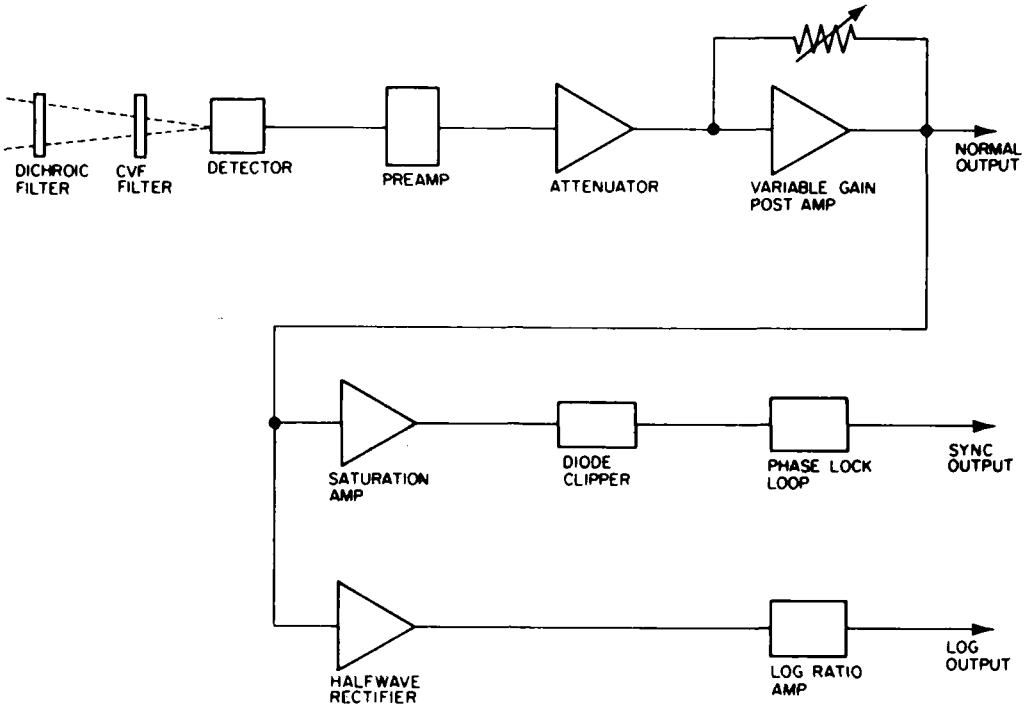

Figure 3. Block Diagram of the Receiver Electronics

$$\frac{V_c}{A_e} \alpha \ M \quad . \tag{2}$$

Multiplying Eq. (2) by the effective area of the collimator, A_c, (cm^2), and dividing by the angular divergence of the source collimator, results in a relationship that is proportional to the radiant intensity of the collimator. The angular divergence of the collimator is the area of the source aperture wheel pinhole of diameter, d_s, which is in place during the calibration, divided by the focal length squared, f^2, of the collimator. Therefore,

2.3 Electronic Design

The 1140 Hz chopped source signal, after detection and preamplification, is sent to a digitally-controlled 10-bit binary attenuation circuit. This circuit can control the attenuation from 1023/1024 down to 3/1024 of the incoming preamp signal. The signal from the attenuator is sent to a variable gain operational amplifier that can be adjusted to provide convenient calibration values. This signal, the normal output, is also sent to the phase lock loop and logarithmic amplifier circuits. The signal that enters the phase lock loop circuit is first amplified to saturation and then clipped by diodes to obtain a constant level signal for the phase lock loop integrated circuit. The phase lock loop further stabilizes the sync output; it is used as the reference phase on an EGG Model 186A Synchro-Het lock-in-amplifier. The dc output of the lock-in-amplifier is directly proportional to the incident radiation falling on the detector.

The signal that enters the logarithmic amplifier circuit is first rectified using a 741 operational amplifier, and then sent to a log ratio amplifier. This log amplifier circuit is used when the incoming radiation is scintillating because of turbulence effects on propagation. Since theory predicts a log-normal probability distribution to this random process, the log amplifier circuit is used in an effort to obtain a more accurate average of transmission. Either the log output or the normal output is then sent to the signal input of the lock-in-amplifier. Then the output of the lock-in-amplifier is either read with a digital voltmeter, or recorded on a strip chart recorder. A block diagram of the receiver electronics is shown in Figure 3.

2.4 Transmissometer Calibration

The collimator aperture diameter is much smaller than the range at which transmission measurements are made. Therefore, the power in Watts, Φ collected by the transmissometer receiver at range, R, is

$$\Phi = \tau I \Omega \quad , \tag{1}$$

where τ is the transmission, I is the radiant intensity of the collimator, and Ω is the solid angle subtended by the receiver at range R. The radiant exitance of the collimator, M (Watts/cm^2), is measured by placing an aperture of area, A_e (cm^2), near the exit pupil of the collimator to stop down the receiver optics. The calibration voltage recorded, V_c, divided by A_e, is proportional to the radiant exitance:

possible to slightly defocus the spot image on each detector and thereby reduce the error by spreading the energy symmetrically over a larger area. However, HgCdTe is typically not uniform, and can vary by 50 percent over its surface. Therefore, it was necessary to install in the HgCdTe detector assembly a field lens. This lens was placed immediately ahead of the detector chip and works by imaging the receiver system entrance pupil (the collector mirror aperture) onto the detector. This is a well known technique used in detector technology and has solved the nonuniformity problems inherent with HgCdTe detectors.

The transmissometer source is a classical Newtonian telescope; 16.5 in. diameter clear aperture with a 49.5 in. focal length. It acts as a collimator to transmit simultaneously the visible and 3- to 14-μm energy (chopped at 1140 Hz) over the range to the receiver site. An optical schematic is shown in Figure 2. An aperture wheel is located at the focus of the primary mirror. The circular apertures contained in this wheel range in diameter from 0.0025 to 0.1404 in. and are used to control the angular divergence of the source radiation and calibrate the transmissometer.

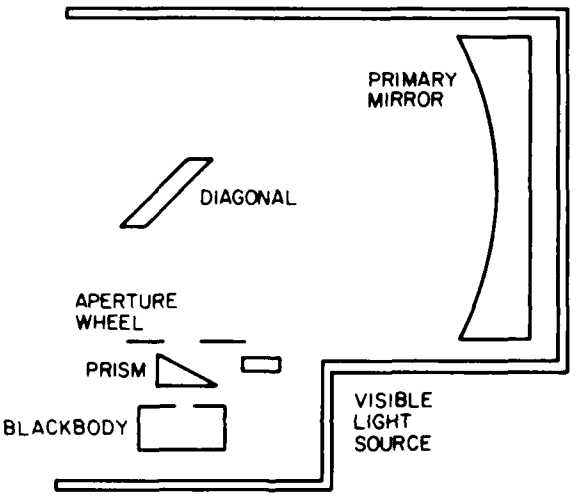

Figure 2. Source Optical Layout

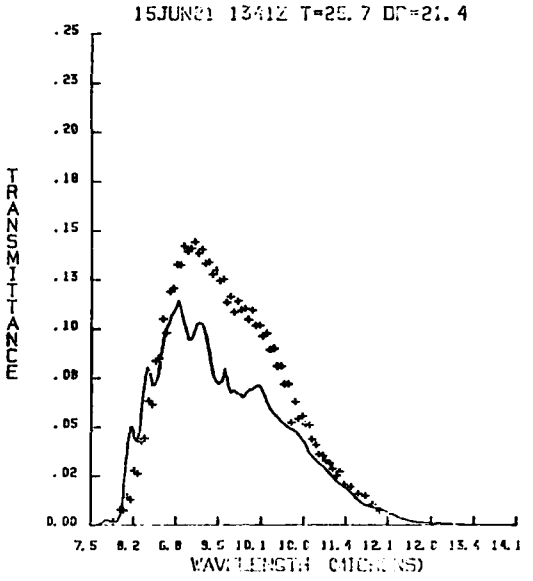

Figure 12. Sample Transmittance Measurements (+) and Calculated LOWTRAN 5 Transmittance Without Aerosols (—) vs Wavelength Under Conditions of High Humidity and Low Visibility 8- to 14-μm Region (15 June 81, 1341Z, 8-km Path)

by aerosols. The transmittance due to various atmospheric absorbers is shown in Figure 13 for conditions representative of the TSCF path. The path length is 8 km, the water vapor density of 10 gm/m^3 represents an average amount for these measurements, and the meteorological range of 50 km represents a clear day. The ozone density of 5.4×10^{-4} gm/m^3 is an average surface value. Plotted separately are the total transmittance and the transmittance due to the water vapor continuum, water vapor band transmittance, and aerosol extinction. In the most transparent regions of the window, the dominant absorber is the water vapor continuum. The aerosol transmittance is high because a high value of the meteorological range was used. The remaining absorbers are the uniformly mixed gases, principally carbon dioxide, nitrogen continuum in the 3- to 5-μm region, and ozone around 1050 cm^{-1}. With the exception of ozone, the absorption by these gases changes very little with meteorological conditions.

To examine the dependence of the measured transmittance on the water vapor amount, three filter positions in the 8- to 12-μm region (10.7, 10.1, and 8.5 μm) and two in the 3- to 5-μm region (3.89 and 4.68 μm) were selected for detailed analysis. Figure 14 (a and b) shows a typical CVF measurement with the selected

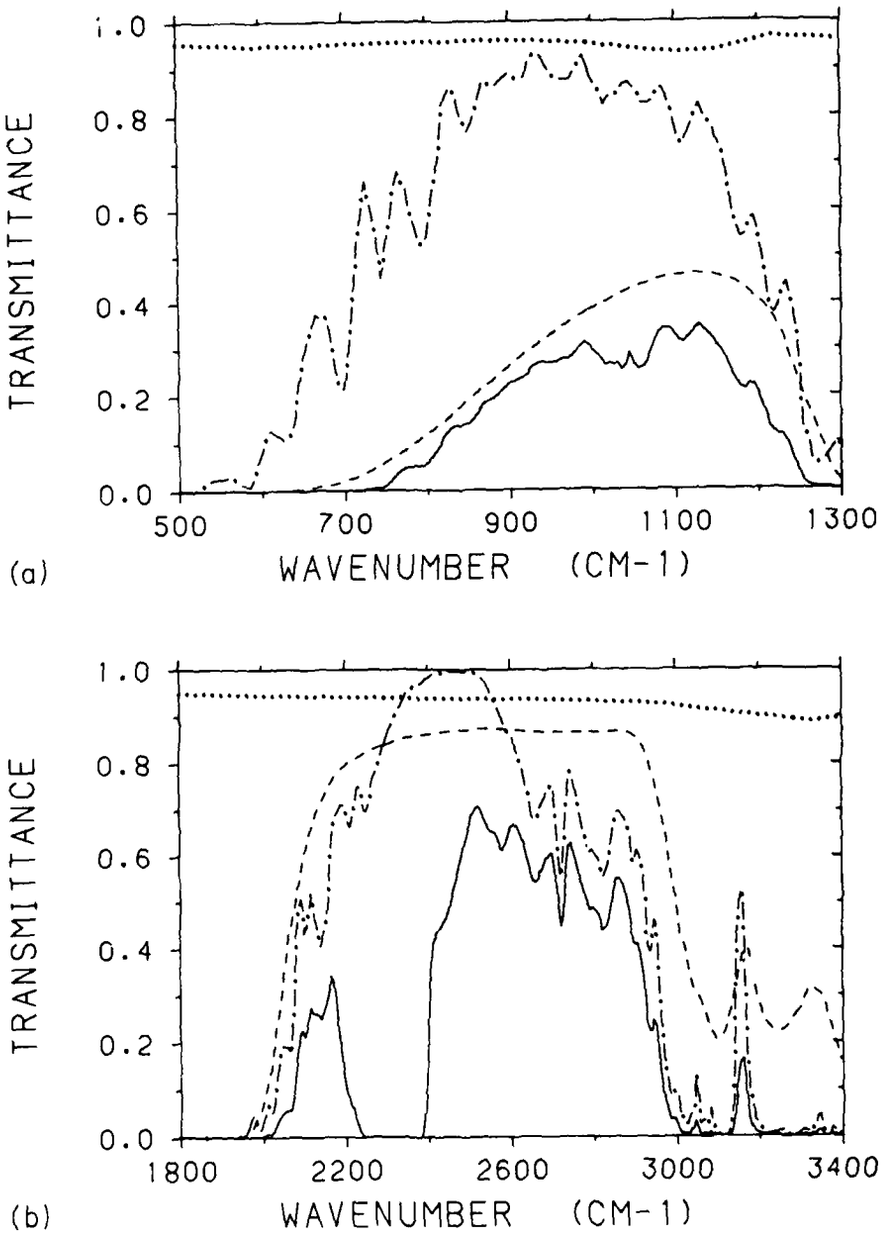

Figure 13. LOWTRAN 6 Calculation of Atmospheric Transmittance for the Conditions: 1013 mb, 296K, 10.0 gm/m^3 Water Vapor, 8-km Path, RURAL Aerosol Model, VIS = 50 km. Solid line is total transmittance, dashed line is water vapor continuum transmittance, dash-dot line is water vapor band transmittance, and dotted line is aerosol transmittance: (a) 500 to 1300 cm^{-1} and (b) 1800 to 3400 cm^{-1}

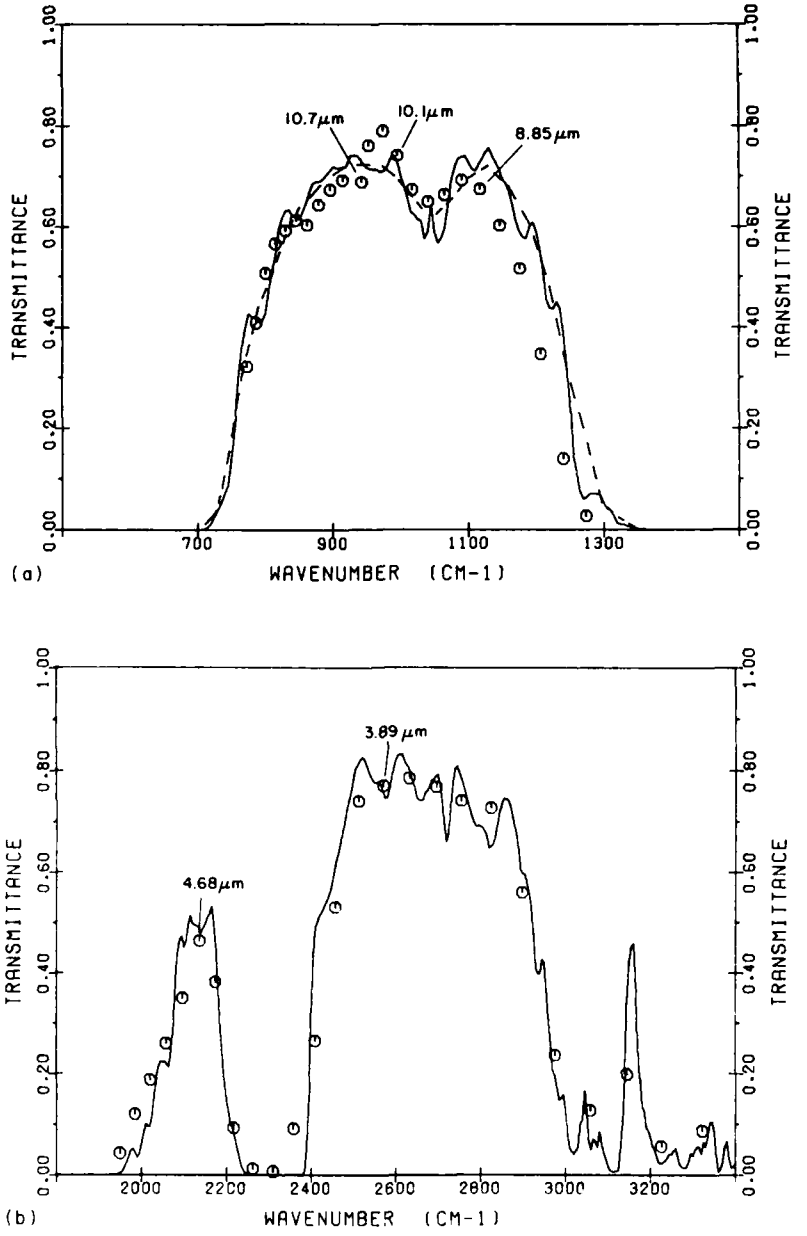

Figure 14. Typical CVF Transmittance Measurement for 8-km (Ⓣ) Path and LOWTRAN Calculation (Solid Line). The filter positions selected for analysis are indicated: (a) 500 to 1500 cm^{-1}. Also shown is LOWTRAN calculation degraded with 6 percent CVF filter (dashed line) (7 May 81, 1433Z, 8-km Path) and (b) 1800 to 3400 cm^{-1} (7 May 81, 1405Z, 8-km Path)

filter positions indicated. Also shown are the LOWTRAN calculations for these cases but with no aerosol extinction included. The filter position at 10.1 μm is slightly affected by the ozone absorption centered at 9.6 μm, while for the filter at 4.68 μm about half of the absorption is due to water vapor band absorption.

The data for each filter position was plotted in both transmittance and optical depth per km vs water vapor density. These plots are shown in Figures 15 through 20. The optical depth per km is actually $-(\ell n \tau)/L$, where τ is the transmittance and L is the path length (either 8 or 2.25 km). Since the transmittance data have been spectrally averaged and do not obey Beer's law, this quantity is not a true optical depth. For this reason, the data for the 8- and 2.25-km paths are plotted separately.

In order to give some indication of the effect of aerosol extinction on the transmittance, the data were divided into three groups according to the observer estimated meteorological range (VIS): high (VIS $\geq$ 15 km, indicated by X), moderate (15 km > VIS $\geq$ 5 km, indicated by ⓞ), and low (VIS < 5 km, indicated by Δ). Aerosol properties are known to change with relative humidity, particularly above 90 percent relative humidity. The effect of relative humidity is considered by plotting separately the data for all relative humidities and relative humidities less than or equal to 90 percent.

Also shown on each plot is the LOWTRAN transmittance or optical depth per km for two temperatures; 286 and 296K. The LOWTRAN 6 calculations do not include the aerosols. The LOWTRAN 6 code contains a new water vapor continuum model extending from 0 to 20,000 cm^{-1}. The continuum contribution from water vapor absorption is expressed in terms of self, and foreign, density-dependent absorption coefficients. The new continuum model in LOWTRAN is described in Appendix C.

3.3 Presentation of the Data

The comparison of the data and the LOWTRAN calculations is presented in Figures 15 through 20. Figure 15 presents the 8- to 12-μm data for the 8-km path. Figure 15 (a), (b), and (c) shows all the data on a transmittance scale. Figure 15 (d), (e), and (f) shows the same data on a log scale. And Figure 15 (g), (h), and (i) shows only the data points for which the relative humidity is less than or equal to 90 percent. No aerosol extinction is included in the LOWTRAN calculation. The measured data is grouped into three categories according to the observer estimated meteorological range, as indicated in the legend.

In a similar fashion, the 8- to 12-μm data for the 2.25-km path is shown in Figure 16. Note again the optical depth per km scale is not a true optical depth, so that the 2.25- and 8-km data cannot be directly compared.

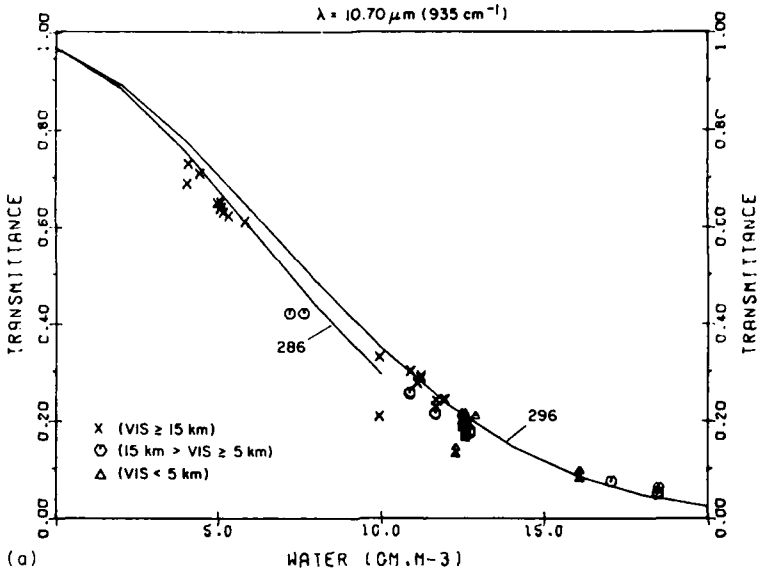

(a) 10.70-μm Filter, Transmittance Scale, All Data

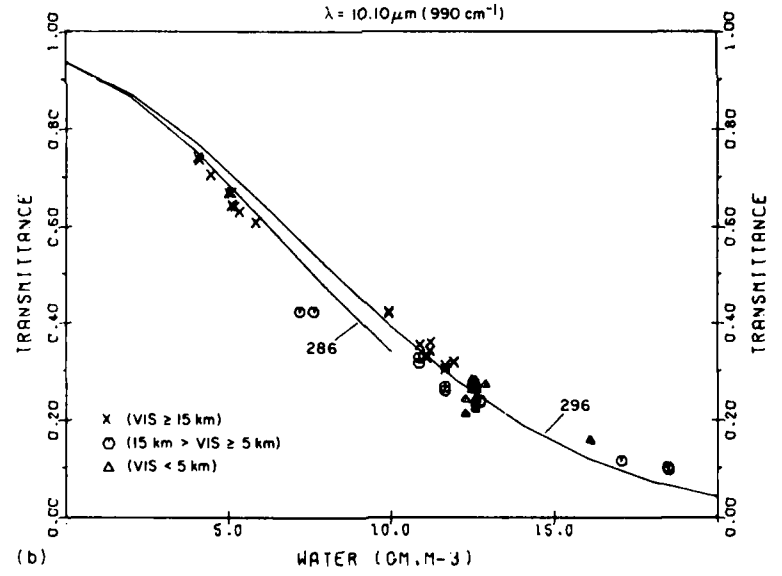

(b) 10.10-μm Filter, Transmittance Scale, All Data

Figure 15. Measured Transmittances (Symbols) and LOWTRAN Calculations (Solid Lines) at 286 and 296K for the 8- to 12-μm Region and the 8-km Path

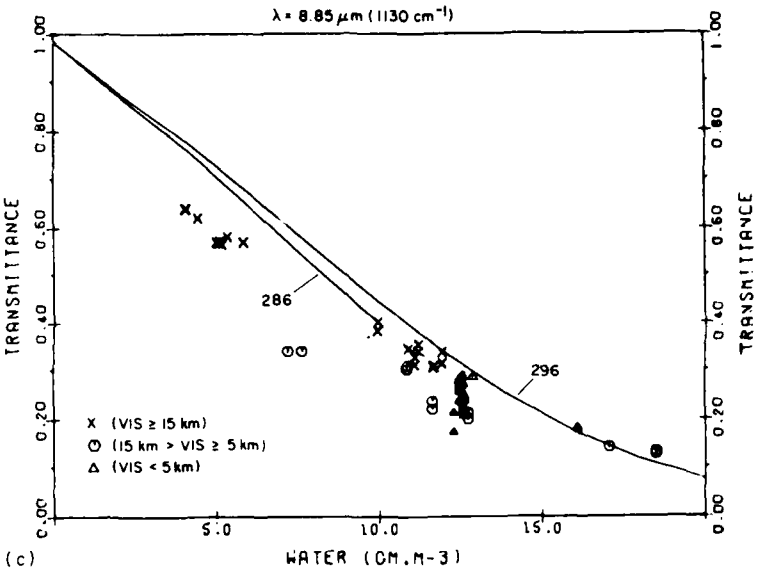

(c) 8.85-μm Filter, Transmittance Scale, All Data

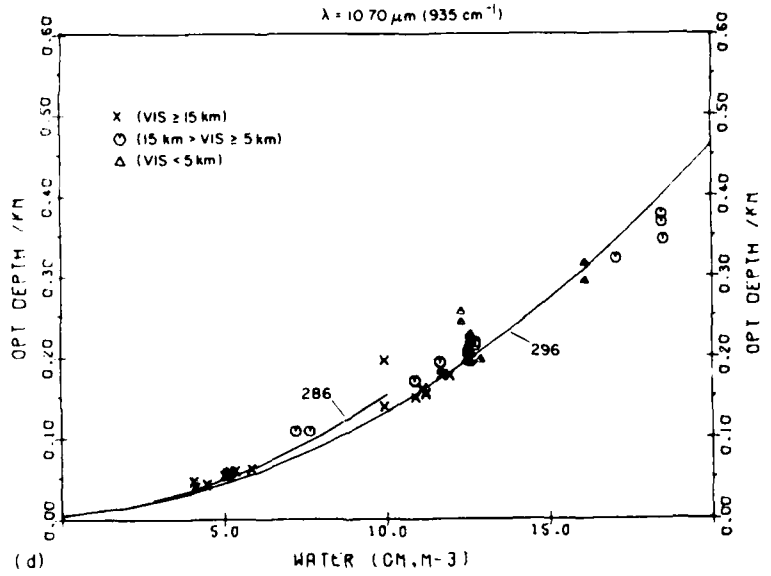

(d) 10.70-μm Filter, Optical Depth/km Scale, All Data

Figure 15. Measured Transmittances (Symbols) and LOWTRAN Calculations (Solid Lines) at 286 and 296K for the 8- to 12-μm Region and the 8-km Path

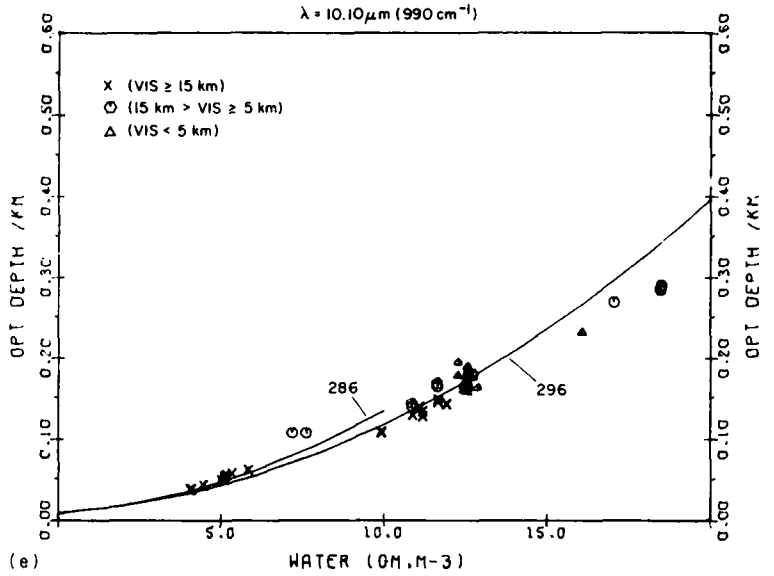

(e) 10.10-μm Filter, Optical Depth/km Scale, All Data

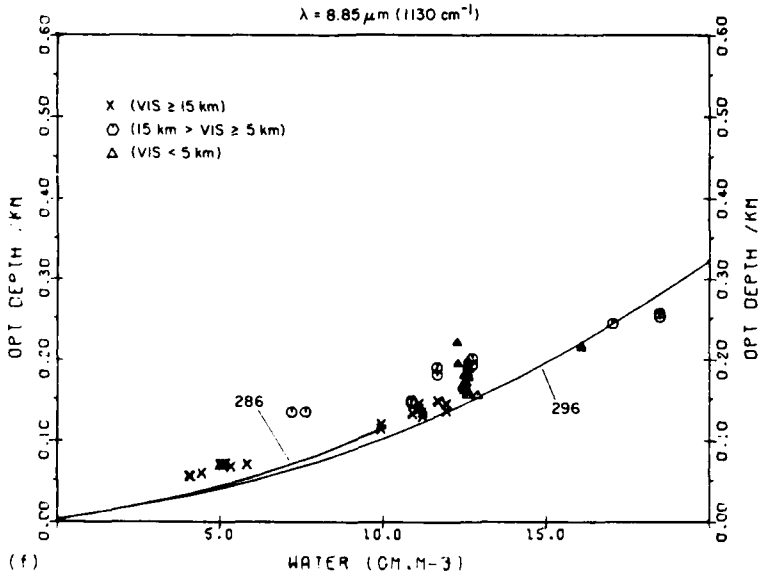

(f) 8.85-μm Filter, Optical Depth/km Scale, All Data

Figure 15. Measured Transmittances (Symbols) and LOWTRAN Calculations (Solid Lines) at 286 and 296K for the 8- to 12-μm Region and the 8-km Path

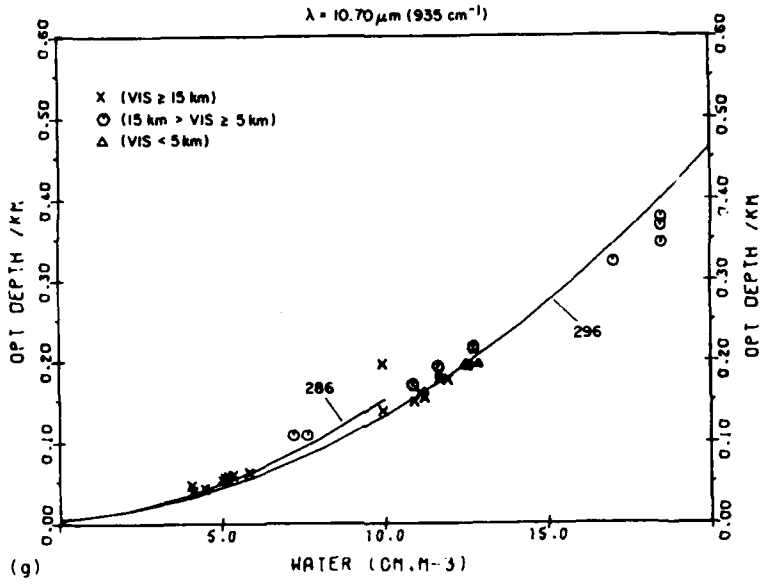

(g) 10.70-μm Filter, Optical Depth/km Scale, RH ≤ 90 percent

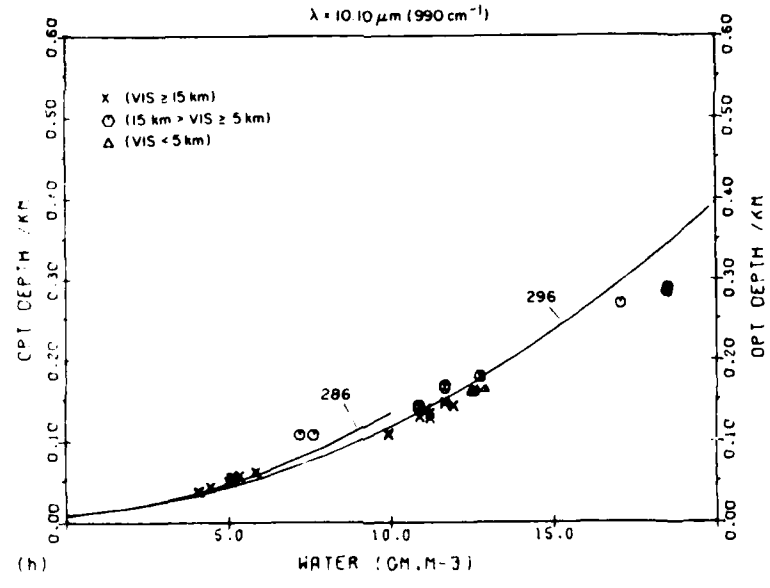

(h) 10.10-μm Filter, Optical Depth/km Scale, RH ≤ 90 percent

Figure 15. Measured Transmittances (Symbols) and LOWTRAN Calculations (Solid Lines) at 286 and 296K for the 8- to 12-μm Region and the 8-km Path

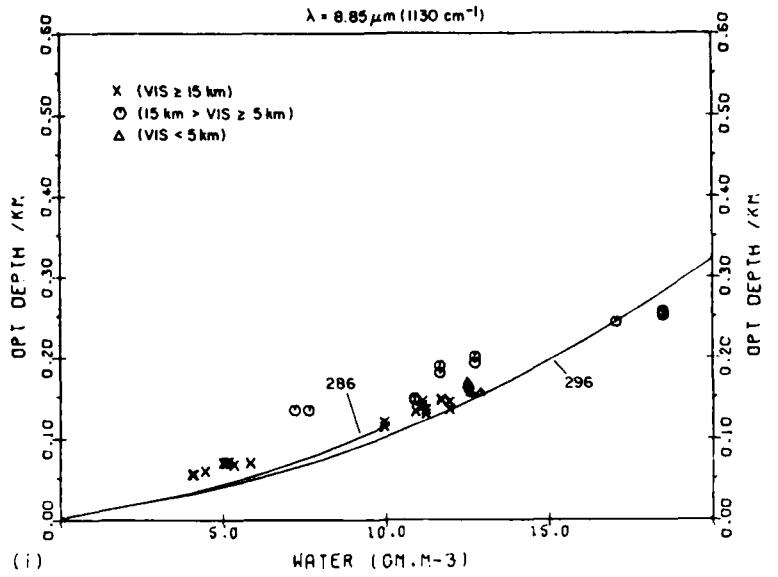

(i) 8.85-μm Filter, Optical Depth/km Scale, RH ≤ 90 percent

Figure 15. Measured Transmittances (Symbols) and LOWTRAN Calculations (Solid Lines) at 286 and 296K for the 8- to 12-μm Region and the 8-km Path

The CVF Transmissometer has a nominal resolution of 6 percent in the 8- to 12-μm region and 2 percent in the 3- to 5-μm region. Figure 17 shows the transmittance of a typical 6 percent CVF centered at about 1075 cm^{-1}. LOWTRAN has a resolution of 20 cm^{-1} (full width at half-maximum).

To test the effect of the greater bandpass of the data, the LOWTRAN calculations at 296K were convolved with the filter functions corresponding to the three selected positions. The results are shown in Figure 18.

In the same way as the 8- to 12-μm data, the data for the two selected filters in the 3- to 5-μm region are shown in Figure 19 (8-km path) and Figure 20 (2.25-km).

3.4 Comments

In the 8- to 12-μm region, the high visibility points (indicated by an X in Figures 15 and 16) agree, with a few exceptions, to within 10 percent in transmittance to the LOWTRAN calculations. One notable exception is the data for the 8.85-μm filter on the 8-km path [Figure 15 (e) and (f)], where the data clustered around 5 gm/m^3 of water vapor is consistently 15 percent less than the LOWTRAN transmittance. The data for the 2.25-km path [Figure 16 (e) and (f)] shows a similar pattern.

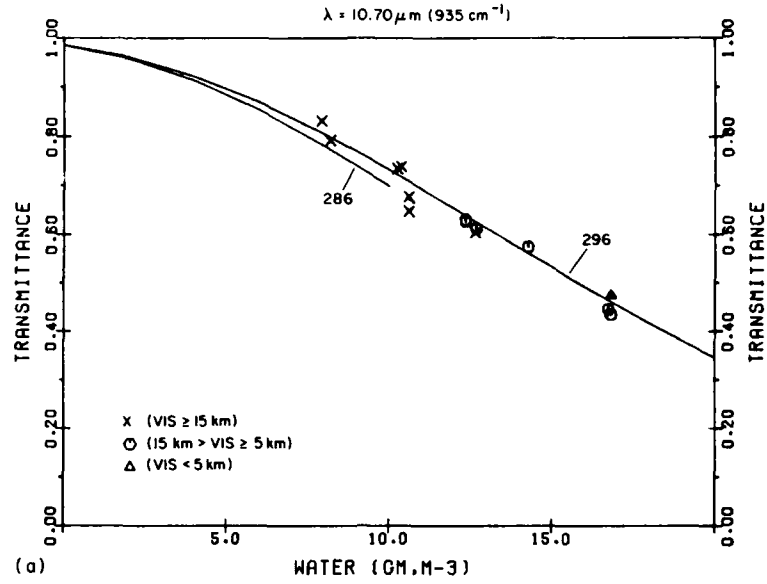

(a) 10.70-μm Filter, Transmittance Scale, All Data

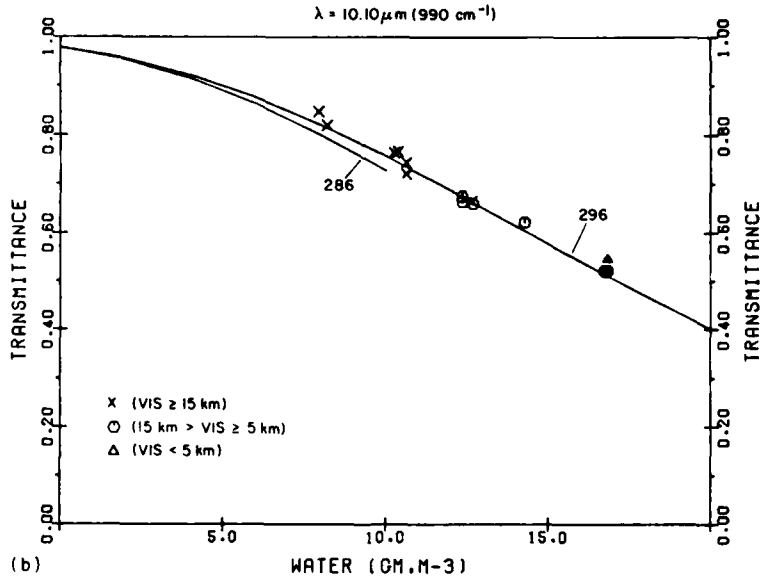

(b) 10.10-μm Filter, Transmittance Scale, All Data

Figure 16. Measured Transmittances (Symbols) and LOWTRAN Calculations (Solid Lines) at 286 and 296K for the 8- to 12-μm Region and the 2.25-km Path

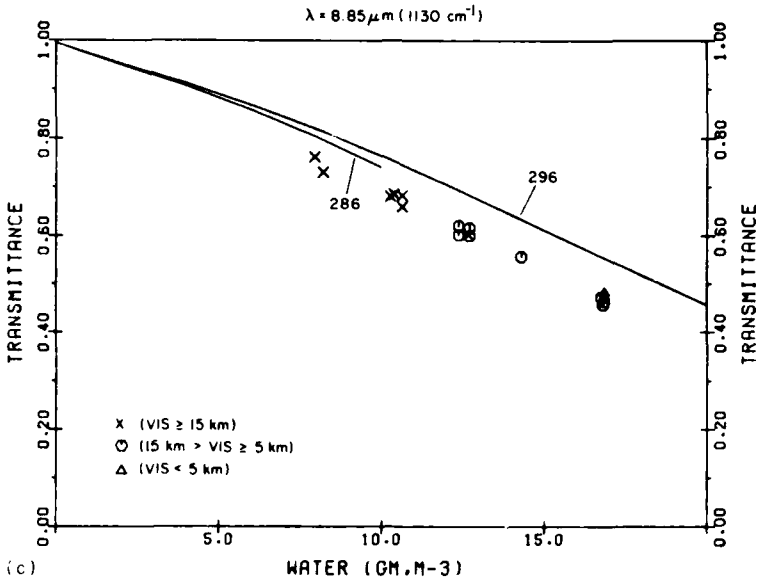

(c) 8.85-μm Filter, Transmittance Scale, All Data

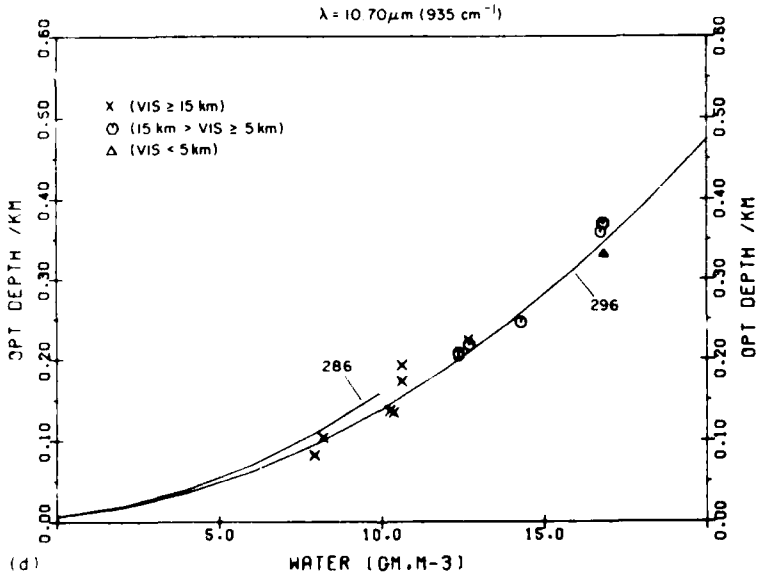

(d) 10.70-μm Filter, Optical Depth/km Scale, All Data

Figure 16. Measured Transmittance (Symbols) and LOWTRAN Calculations (Solid Lines) at 286 and 296K for the 8- to 12-μm Region and the 2.25-km Path

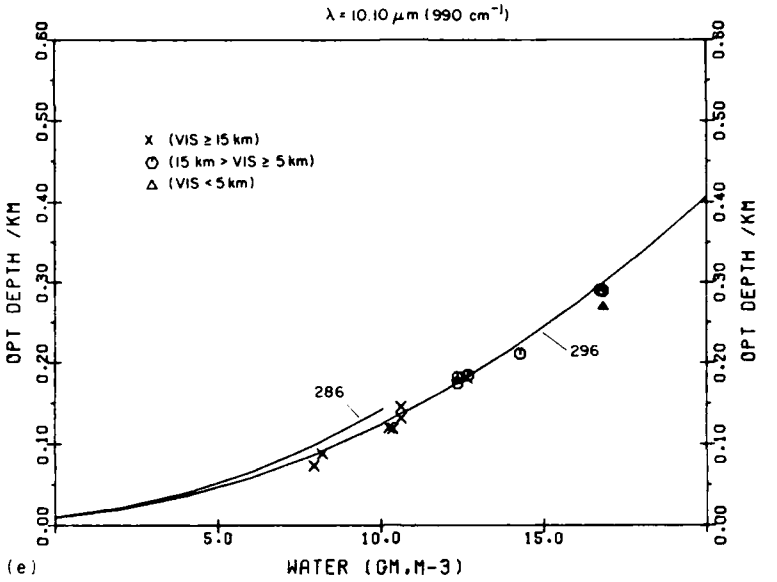

(e) 10.10-μm Filter, Optical Depth/km Scale, All Data

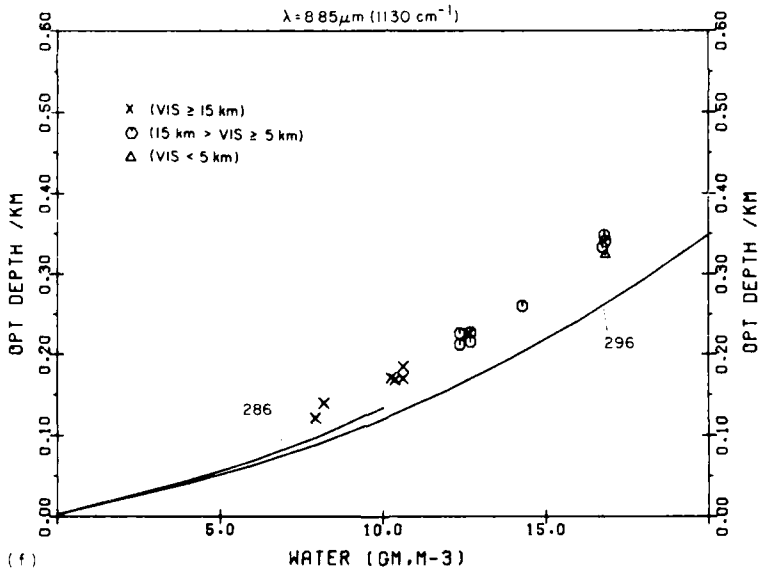

(f) 8.85-μm Filter, Optical Depth/km Scale, All Data

Figure 16. Measured Transmittances (Symbols) and LOWTRAN Calculations (Solid Lines) at 286 and 296K for the 8- to 12-μm Region and the 2.25-km Path

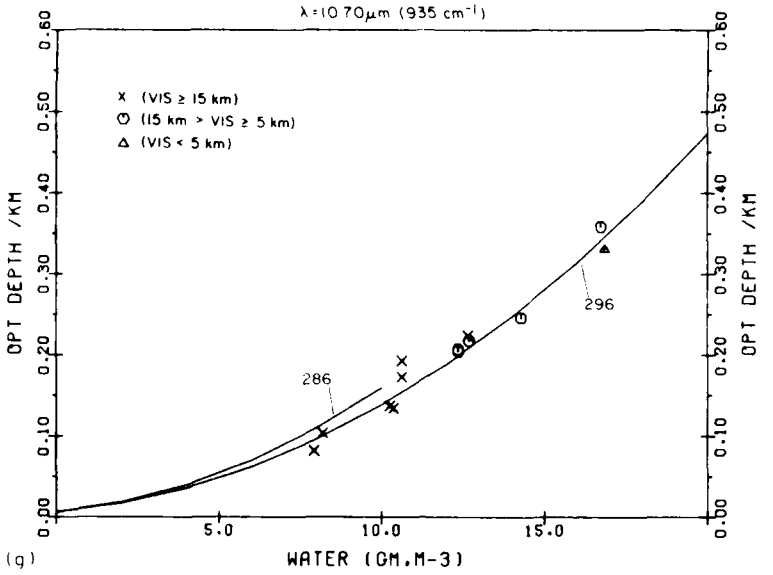

(g) 10.70-μm Filter, Optical Depth/km Scale, RH ≤ 90 percent

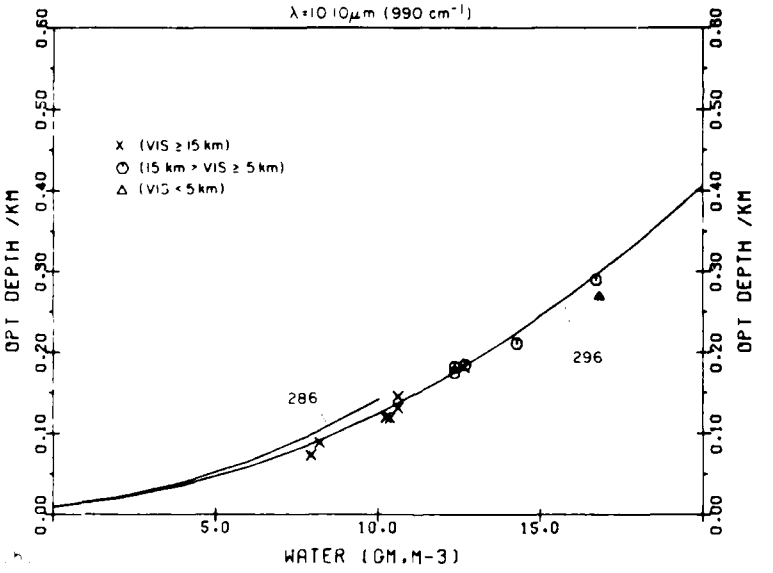

(h) 10.10-μm Filter, Optical Depth/km Scale, RH ≤ 90 percent

Figure 16. Measured Transmittance (Symbols) and LOWTRAN Calculations (Solid Lines) at 286 and 296K for the 8- to 12-μm Region and the 2.25-km Path

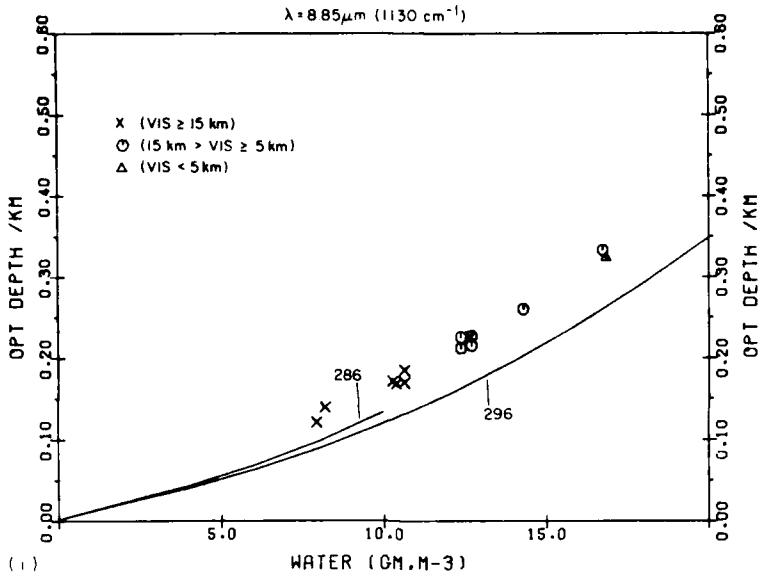

(i) 8.85-μm Filter, Optical Depth/km Scale, RH ≤ 90 percent

Figure 16. Measured Transmittance (Symbols) and LOWTRAN Calculations (Solid Lines) at 286 and 296K for the 8- to 12-μm Region and the 2.25-km Path

Considering the moderate and low visibility data (indicated by ⏀ and Δ), the remarkable point is not that some of the data does not fit the LOWTRAN calculation but rather that so much of the data still tracks LOWTRAN calculated without aerosols. A few points even indicate less extinction than LOWTRAN. Special note should be made of the data taken almost continuously on 28 May between 1124 to 1936 (the data itself is listed in Appendix A with the observer's comments in Appendix B). Haze and fog with light drizzle conditions existed up to 1330, with observer estimated visibility at 2 to 4 km after the rain ended. During this period, the absolute humidity remained approximately constant at 12.5 gm/m^3, while the relative humidity decreased from 100 percent during the fog, to 80 percent at the conclusion of the experiment. In spite of the low visibility, none of the data points around 12.5 gm/m^3 are significantly above the LOWTRAN calculation.

On the 8-km path are five data points that exceed 15 gm/m^3 of water vapor. In the 8- to 12-μm region [see Figure 15 (d), (e), and (f)] most of these data points show less extinction than predicted by LOWTRAN. A comparable effect is not seen in the data for the 2.25-km path.

Table A2. Listing of CVF Transmissometer and Meteorological Data: 3- to 5-μm (Contd)

DATE	8KM PATH TIME	T(C)	TD(C)	TRANS AT 4.6	3.9	4.68	VIS	RH	H2O
24 JUNE	1107	18.07	13.57	.235	.636	.232	80.00	74.57	11.561
24 JUNE	1211	19.80	14.26	.250	.723	.253	80.00	69.68	12.019
RANGE CHANGED TO 2.25 KM AT THIS POINT									
22 JULY	1321	18.80	16.50	.510	.860	.523	15.00	88.23	13.927
23 JULY	1754	21.19	11.60	.550	.800	.597	25.00	54.34	10.184
24 JULY	1501	23.00	15.53	.539	.659	.514	30.00	62.09	12.904
29 JULY	1410	14.94	12.20	.558	.865	.549	25.00	83.41	10.683
11 AUG	1424	21.16	16.70	.500	.650	.508	10.00	75.19	13.992
13 AUG	1447	21.96	17.32	.473	.825	.456	13.00	74.43	14.514
14 AUG	1251	22.20	19.70	.394	.781	.376	4.00	85.40	16.636
17 AUG	1816	20.50	7.90	.550	.837	.614	30.00	43.56	7.058
17 AUG	1825	20.60	7.67	.580	.870	.647	30.00	42.60	7.734

Table A2. Listing of CVF Transmissometer and Meteorological Data: 3- to 5-μm

DATE	6KM PATH TIME	T(C)	TD(C)	TRANS AT 4.6	3.9	4.66	VIS	RH	H2O
7 MAY	1337	7.60	-1.00	.283	.764	.468	70.00	54.17	4.384
7 MAY	1352	7.73	-1.25	.292	.753	.479	70.00	52.71	4.302
7 MAY	1405	7.70	-1.30	.292	.753	.479	70.00	52.62	4.287
7 MAY	1405	8.01	-1.63	.282	.771	.464	70.00	51.27	4.180
7 MAY	1417	8.00	-1.60	.282	.771	.464	70.00	51.42	4.189
8 MAY	1156	6.72	-1.27	.328	.690	.414	50.00	54.44	4.311
8 MAY	1212	6.73	-1.30	.328	.690	.414	50.00	54.40	4.302
8 MAY	1231	7.95	-.43	.350	.696	.426	50.00	55.14	4.564
8 MAY	1247	8.00	-.40	.350	.698	.426	50.00	55.06	4.574
8 MAY	1249	9.39	.19	.334	.717	.405	50.00	52.28	4.751
8 MAY	1313	9.40	.20	.334	.717	.405	50.00	52.29	4.754
8 MAY	1406	11.40	2.14	.333	.726	.389	50.00	52.56	5.427
8 MAY	1422	11.40	2.10	.333	.726	.389	50.00	52.41	5.412
8 MAY	1424	12.10	2.40	.350	.714	.400	50.00	51.10	5.515
11 MAY	1248	12.90	12.60	.093	.373	.095	3.00	96.02	11.046
12 MAY	1702	11.20	3.20	.334	.682	.365	60.00	57.47	5.656
12 MAY	1740	12.10	3.70	.334	.661	.370	60.00	56.06	6.047
19 MAY	1325	8.90	1.60	.329	.658	.372	25.00	55.69	5.266
19 MAY	1416	9.60	1.20	.339	.694	.381	25.00	55.47	5.106
20 MAY	1336	13.20	1.20	.318	.651	.357	35.00	48.59	5.042
20 MAY	1352	14.10	1.95	.327	.676	.374	35.00	48.32	5.304
22 MAY	1328	17.40	8.60	.169	.630	.266	10.00	55.71	8.329
27 MAY	1700	19.50	17.00	.100	.242	.104	6.00	85.17	14.342
28 MAY	1124	14.30	14.30	.126	.260	.130	4.00	101.00	12.261
28 MAY	1158	14.20	14.20	.073	.154	.074	4.00	101.00	12.206
28 MAY	1408	14.80	14.60	.205	.526	.204	4.00	96.65	12.500
28 MAY	1440	15.20	14.60	.213	.589	.212	4.00	96.14	12.483
28 MAY	1540	15.20	14.50	.196	.539	.197	4.00	95.51	12.402
28 MAY	1617	15.60	14.60	.197	.526	.196	4.00	92.44	12.457
28 MAY	1806	17.50	14.60	.225	.635	.223	4.00	83.85	12.545
28 MAY	1911	17.60	15.00	.226	.654	.218	4.00	84.45	12.703
2 JUNE	1521	19.20	18.90	.171	.561	.159	4.00	96.10	16.182
2 JUNE	1602	19.70	19.00	.173	.577	.156	4.00	95.64	16.256
11 JUNE	1250	18.70	13.70	.175	.566	.180	12.00	72.24	11.634
11 JUNE	1305	18.80	13.90	.194	.667	.207	12.00	72.73	11.782
11 JUNE	1402	20.20	14.10	.225	.654	.233	12.00	67.41	11.679
12 JUNE	1817	24.90	20.70	.090	.490	.111	12.00	76.93	17.749
15 JUNE	1319	25.80	21.40	.146	.537	.126	12.00	76.07	18.474
15 JUNE	1423	26.70	21.70	.144	.536	.123	12.00	73.36	18.761
15 JUNE	1438	26.70	21.50	.144	.536	.123	12.00	72.44	18.532
17 JUNE	1311	15.40	11.20	.273	.666	.260	45.00	75.69	9.564
17 JUNE	1349	16.00	11.10	.300	.701	.305	45.00	72.30	9.697
19 JUNE	1233	20.00	14.50	.165	.596	.165	8.00	71.09	12.199
19 JUNE	1335	21.90	14.50	.177	.670	.180	6.00	62.17	12.121
19 JUNE	1435	22.90	14.60	.194	.604	.194	8.00	58.78	12.158
22 JUNE	1615	21.80	13.60	.237	.653	.237	60.00	56.56	11.437
22 JUNE	1735	22.17	13.18	.271	.655	.259	60.00	54.02	11.114
22 JUNE	1740	21.80	13.60	.271	.655	.259	60.00	56.56	11.437
23 JUNE	1138	17.19	14.16	.214	.648	.219	80.00	82.06	12.049
23 JUNE	1154	17.20	14.20	.214	.648	.219	80.00	82.22	12.080
23 JUNE	1240	18.66	14.06	.237	.669	.238	60.00	74.16	11.911
23 JUNE	1258	18.20	14.10	.237	.669	.238	60.00	76.59	11.961
23 JUNE	1259	18.36	14.06	.260	.720	.286	80.00	75.60	11.923
24 JUNE	159	21.78	14.06	.225	.606	.227	60.00	61.85	11.785

Table A1. Listing of CVF Transmissometer and Meteorological Data: 8- to 12-μm (Contd)

DATE	8KM PATH TIME	T(C)	TD(C)	TRANS AT 8.65	10.10	10.70	VIS	RH	H2O
28 MAY	1936	19.00	15.30	.287	.272	.209	4.00	78.73	12.669
2 JUNE	1507	18.90	18.00	.181	.158	.096	4.00	98.36	16.058
2 JUNE	1536	19.00	18.60	.177	.157	.060	4.00	96.73	16.092
11 JUNE	1342	19.40	12.70	.313	.316	.235	12.00	64.64	10.872
11 JUNE	1368	19.40	12.70	.310	.326	.256	12.00	64.64	10.872
12 JUNE	1730	25.70	20.10	.142	.116	.076	12.00	70.50	17.057
15 JUNE	1341	25.70	21.40	.128	.103	.049	12.00	76.54	18.481
15 JUNE	1417	25.70	21.40	.133	.101	.053	12.00	76.54	18.481
15 JUNE	1440	27.10	21.50	.132	.098	.063	12.00	70.70	18.907
17 JUNE	1232	14.70	11.10	.363	.423	.209	45.00	78.71	9.942
17 JUNE	1307	14.70	11.10	.401	.419	.331	45.00	78.71	9.942
19 JUNE	1310	20.70	15.20	.213	.240	.160	8.00	70.20	12.732
19 JUNE	1333	20.70	15.20	.210	.236	.175	8.00	70.20	12.732
19 JUNE	1359	22.00	13.90	.220	.260	.215	8.00	59.39	11.654
19 JUNE	1431	22.00	13.90	.236	.265	.213	8.00	59.39	11.654
22 JUNE	1634	21.90	13.30	.354	.359	.292	80.00	57.43	11.212
22 JUNE	1731	21.90	13.30	.340	.342	.268	80.00	57.43	11.212
22 JUNE	1803	22.50	12.90	.345	.354	.302	80.00	53.86	10.900
23 JUNE	1203	17.80	14.06	.314	.316	.242	80.00	78.37	11.946
23 JUNE	1234	17.80	14.06	.338	.319	.244	80.00	78.37	11.946
24 JUNE	124	22.27	13.16	.312	.327	.278	80.00	55.67	11.110
24 JUNE	155	22.27	13.16	.328	.333	.276	80.00	55.67	11.110
24 JUNE	1135	18.80	13.77	.316	.312	.242	80.00	72.11	11.663
24 JUNE	1208	18.80	13.77	.310	.304	.229	80.00	72.11	11.663
RANGE CHANGED TO 2.25 KM AT THIS POINT**********									
22 JULY	1300	18.70	15.00	.662	.665	.604	15.00	78.69	12.656
23 JULY	1306	21.15	11.90	.681	.764	.735	25.00	54.85	10.253
23 JULY	1836	21.68	12.10	.685	.766	.739	25.00	53.76	10.371
24 JULY	1430	22.60	14.84	.662	.675	.631	12.00	60.85	12.361
24 JULY	1435	22.60	14.84	.621	.664	.627	12.00	60.85	12.361
24 JULY	1515	23.54	15.30	.660	.660	.613	12.00	59.14	12.692
24 JULY	1535	23.54	15.30	.616	.660	.612	12.00	59.14	12.692
29 JULY	1342	14.70	12.10	.660	.744	.678	25.00	84.17	10.822
29 JULY	1342	14.70	12.10	.663	.721	.648	25.00	84.17	10.822
4 AUG	1200	20.40	19.60	.465	.522	.435	8.00	95.05	16.635
4 AUG	1230	21.00	19.60	.457	.520	.438	8.00	91.51	16.810
4 AUG	1714	25.80	19.80	.473	.521	.446	10.00	68.75	16.737
13 AUG	1433	21.50	17.04	.557	.622	.575	13.00	75.24	14.261
14 AUG	1238	22.20	19.70	.483	.546	.475	4.00	85.40	16.836
17 AUG	1757	19.90	8.00	.762	.846	.832	30.00	45.56	7.922
17 AUG	1806	20.30	8.50	.731	.822	.792	30.00	45.97	8.191

Table A1. Listing of CVF Transmissometer and Meteorological Data: 8- to 12-μm

DATE	6KM PATH TIME	T(C)	TD(C)	TRANS AT 8.85	10.10	10.70	VIS	RH	H2O
7 MAY	1433	8.66	-2.00	.640	.742	.689	70.00	46.78	4.058
7 MAY	1452	8.87	-1.55	.640	.737	.750	70.00	46.63	4.100
8 MAY	1213	7.29	-.60	.620	.707	.710	50.00	56.17	4.453
8 MAY	1320	9.87	.92	.570	.670	.650	50.00	53.36	5.000
8 MAY	1338	10.30	1.20	.570	.670	.650	50.00	52.89	5.094
12 MAY	1801	12.10	3.20	.570	.609	.611	60.00	54.10	5.638
19 MAY	1346	9.40	1.20	.572	.645	.640	25.00	56.23	5.110
19 MAY	1405	9.30	1.10	.569	.644	.636	25.00	56.20	5.075
19 MAY	1430	9.70	1.40	.565	.641	.629	25.00	55.69	5.178
20 MAY	1258	11.10	1.90	.562	.631	.622	35.00	52.71	5.341
22 MAY	1401	20.80	6.64	.340	.423	.421	10.00	39.17	7.202
22 MAY	1401	19.63	7.42	.340	.423	.421	10.00	44.53	7.626
28 MAY	1139	14.70	14.70	.228	.242	.170	4.00	100.00	12.566
28 MAY	1139	14.70	14.70	.220	.231	.170	4.00	100.00	12.566
28 MAY	1255	14.30	14.30	.172	.231	.130	4.00	100.00	12.261
28 MAY	1255	14.30	14.30	.212	.241	.164	4.00	100.00	12.261
28 MAY	1310	14.70	14.70	.206	.220	.163	4.00	100.00	12.566
28 MAY	1310	14.70	14.70	.211	.224	.166	4.00	100.00	12.566
28 MAY	1310	14.70	14.70	.216	.231	.173	4.00	100.00	12.566
28 MAY	1310	14.70	14.70	.216	.232	.173	4.00	100.00	12.566
28 MAY	1310	14.70	14.70	.219	.235	.175	4.00	100.00	12.566
28 MAY	1335	14.70	14.70	.221	.239	.178	4.00	100.00	12.566
28 MAY	1337	14.90	14.70	.233	.259	.178	4.00	98.70	12.577
28 MAY	1356	14.80	14.60	.254	.261	.163	4.00	98.69	12.500
28 MAY	1356	14.80	14.60	.257	.264	.167	4.00	98.69	12.500
28 MAY	1407	14.80	14.60	.257	.266	.165	4.00	98.69	12.500
28 MAY	1425	15.20	14.60	.270	.270	.195	4.00	96.14	12.483
28 MAY	1425	15.20	14.60	.271	.274	.197	4.00	96.14	12.483
28 MAY	1437	15.20	14.60	.276	.275	.199	4.00	96.14	12.483
28 MAY	1455	15.50	14.70	.275	.276	.197	4.00	94.89	12.551
28 MAY	1455	15.50	14.70	.275	.275	.197	4.00	94.89	12.551
28 MAY	1455	15.50	14.70	.272	.271	.195	4.00	94.89	12.551
28 MAY	1524	15.50	14.60	.256	.267	.193	4.00	94.27	12.470
28 MAY	1524	15.50	14.60	.261	.267	.195	4.00	94.27	12.470
28 MAY	1537	15.50	14.60	.264	.270	.195	4.00	94.27	12.470
28 MAY	1552	15.30	14.60	.230	.260	.167	4.00	95.51	12.479
28 MAY	1552	15.30	14.60	.236	.260	.167	4.00	95.51	12.479
28 MAY	1625	15.70	14.60	.239	.261	.197	4.00	94.28	12.623
28 MAY	1625	15.70	14.60	.242	.264	.199	4.00	94.28	12.623
28 MAY	1637	15.70	14.60	.249	.265	.201	4.00	94.28	12.623
28 MAY	1656	16.60	14.70	.266	.275	.209	4.00	88.34	12.503
28 MAY	1656	16.60	14.70	.268	.277	.209	4.00	88.34	12.503
28 MAY	1708	16.60	14.70	.271	.275	.211	4.00	89.34	12.503
28 MAY	1724	17.00	14.70	.263	.277	.211	4.00	86.06	12.466
28 MAY	1724	17.00	14.70	.262	.275	.209	4.00	86.08	12.466
28 MAY	1738	17.00	14.70	.258	.275	.211	4.00	86.08	12.466
28 MAY	1752	17.40	14.70	.266	.278	.212	4.00	83.88	12.469
28 MAY	1804	17.40	14.70	.268	.275	.211	4.00	83.88	12.469
28 MAY	1827	17.40	14.70	.269	.277	.213	4.00	83.86	12.469
28 MAY	1827	17.40	14.70	.272	.280	.214	4.00	83.86	12.469
28 MAY	1827	17.40	14.70	.281	.282	.211	4.00	83.88	12.469
28 MAY	1855	17.00	14.60	.290	.282	.215	4.00	86.64	12.567
28 MAY	1855	17.00	14.60	.287	.281	.211	4.00	86.64	12.567
28 MAY	1928	17.70	14.90	.287	.272	.209	4.00	83.36	12.618

Appendix A

Listing of Transmissometer and Meteorological Data

A listing of the digitized data used for analysis in Section 3 is presented in this Appendix. The data, shown in Tables A1 and A2, were taken from 7 May to 17 August 1981. Measurements for both the 8- and 2.25-km paths are included. Table A1 lists CVF transmissometer and meteorological data in the 8- to 12-μm region: Table A2 is for the 3- to 5-μm region. As indicated by the header in each table, the digitized values for each measurement are the following: the date, the time, the ambient temperature (°C), the dew point temperature (°C), transmittances at three wavelengths (μm), observer estimated visibility (km), relative humidity (%), and absolute humidity (gm/m^3).

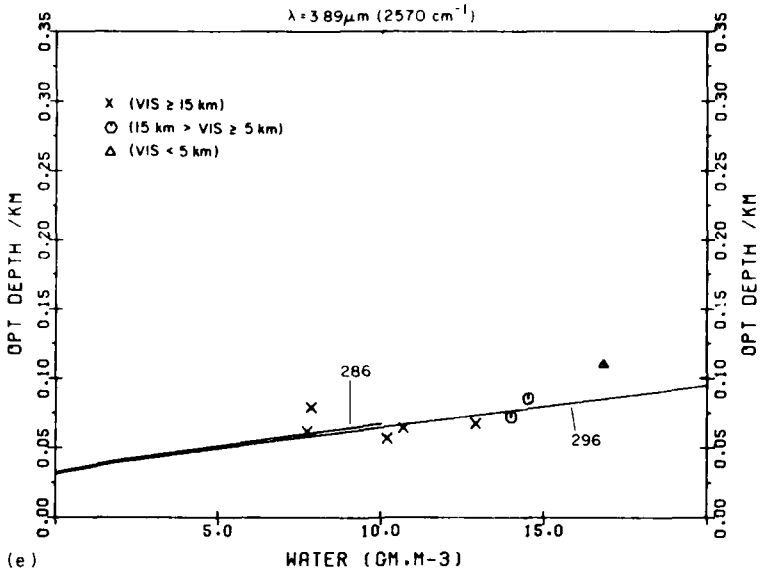

(e) 3.89-μm, Optical Depth/km Scale, RH ≤ 90 percent

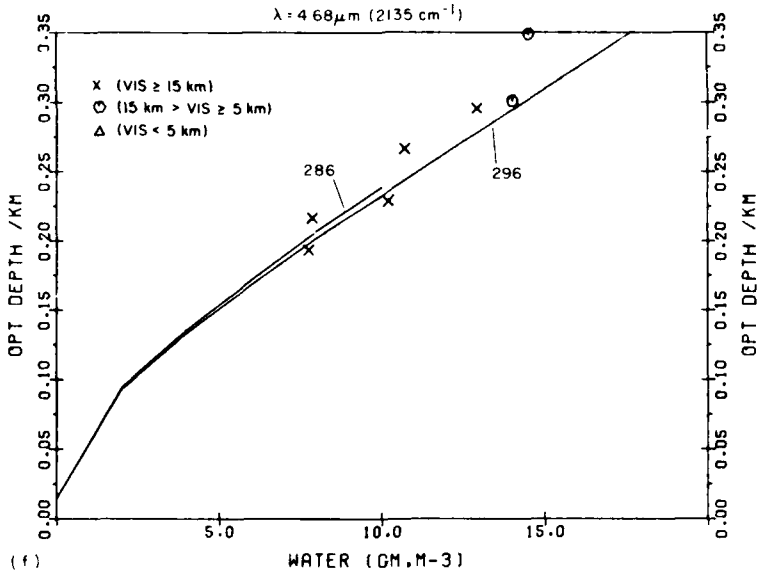

(f) 4.68-μm, Optical Depth/km Scale, RH ≤ 90 percent

Figure 20. Measured Transmittances (Symbols) and LOWTRAN Calculations (Solid Lines) at 286 and 296K for the 3- to 5-μm Region and the 2.25-km Path

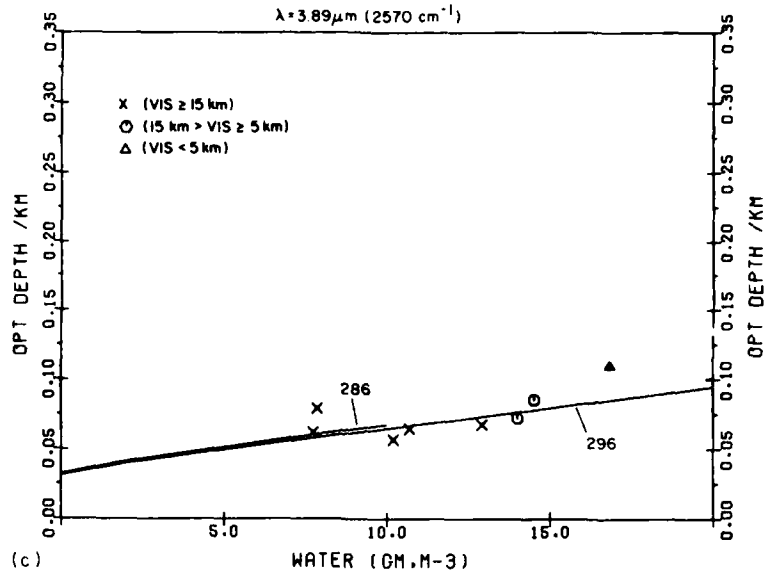

(c) 3.89-μm, Optical Depth/km Scale, All Data

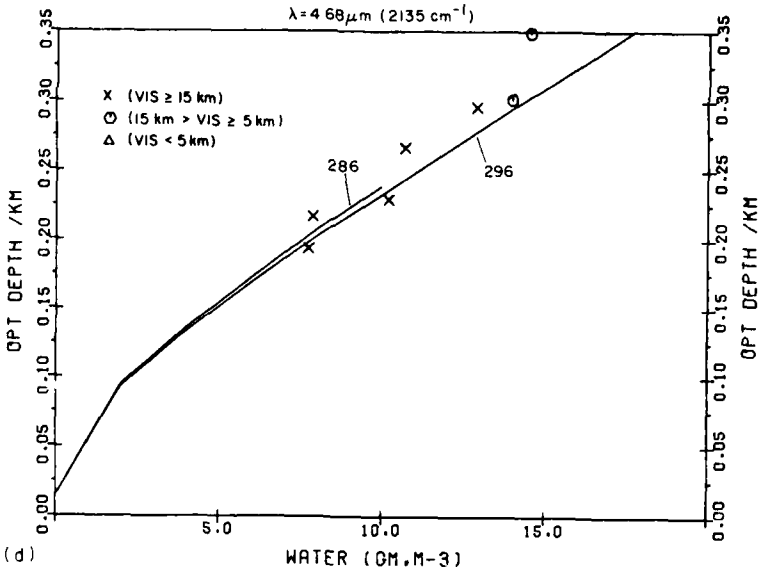

(d) 4.68-μm, Optical Depth/km Scale, All Data

Figure 20. Measured Transmittances (Symbols) and LOWTRAN Calculations (Solid Lines) at 286 and 296K for the 3- to 5-μm Region and the 2.25-km Path

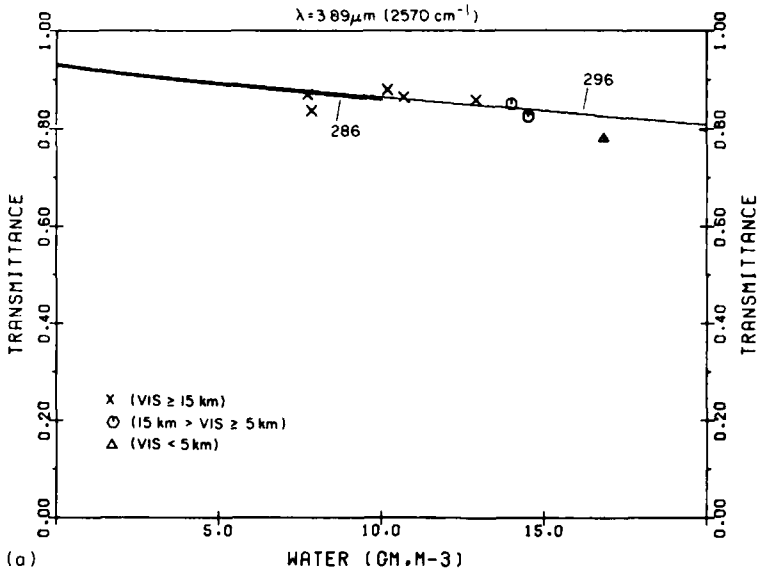

(a) 3.89-μm, Transmittance Scale, All Data

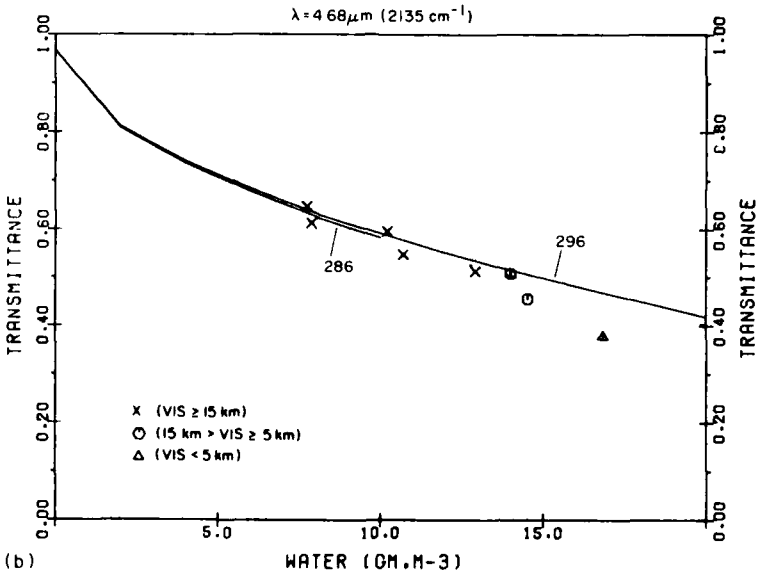

(b) 4.68-μm, Transmittance Scale, All Data

Figure 20. Measured Transmittances (Symbols) and LOWTRAN Calculations (Solid Lines) at 286 and 296K for the 3- to 5-μm Region and the 2.25-km Path

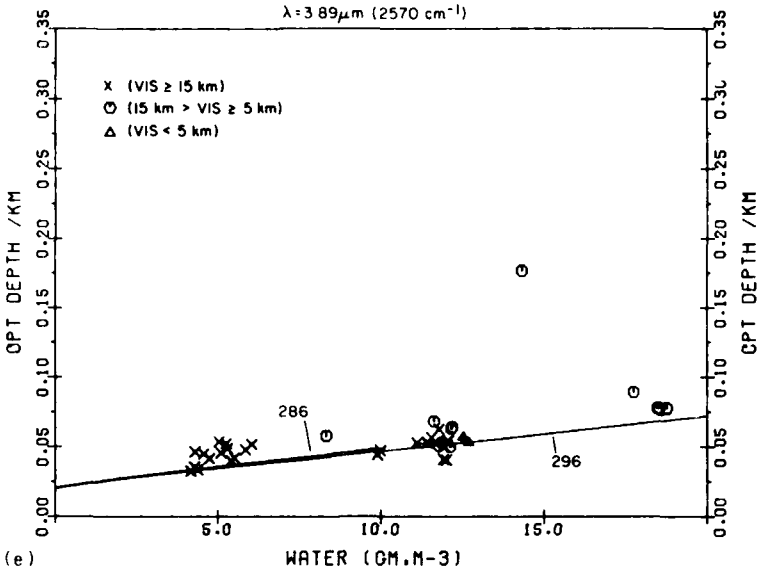

(e) 3.89-μm, Optical Depth/km Scale, RH ≤ 90 percent

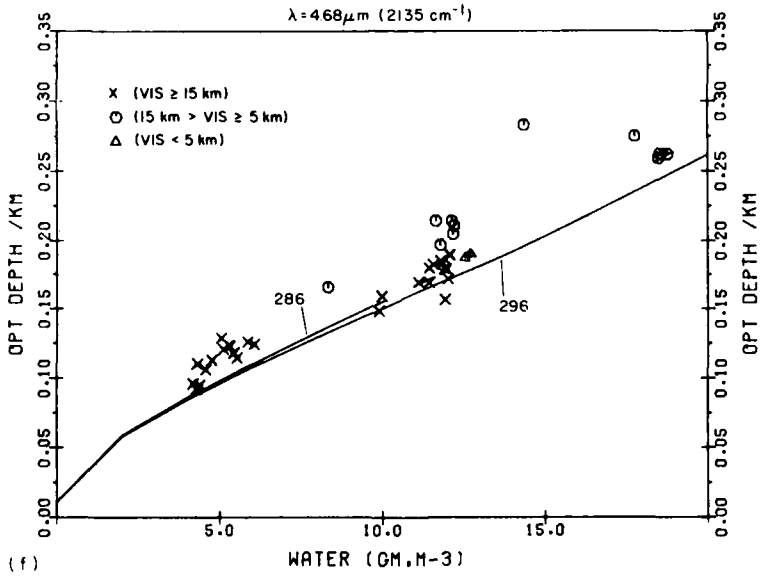

(f) 4.68-μm, Optical Depth/km Scale, RH ≤ 90 percent

Figure 19. Measured Transmittances (Symbols) and LOWTRAN Calculations (Solid Lines) at 286 and 296K for the 3- to 5-μm Region and the 8-km Path

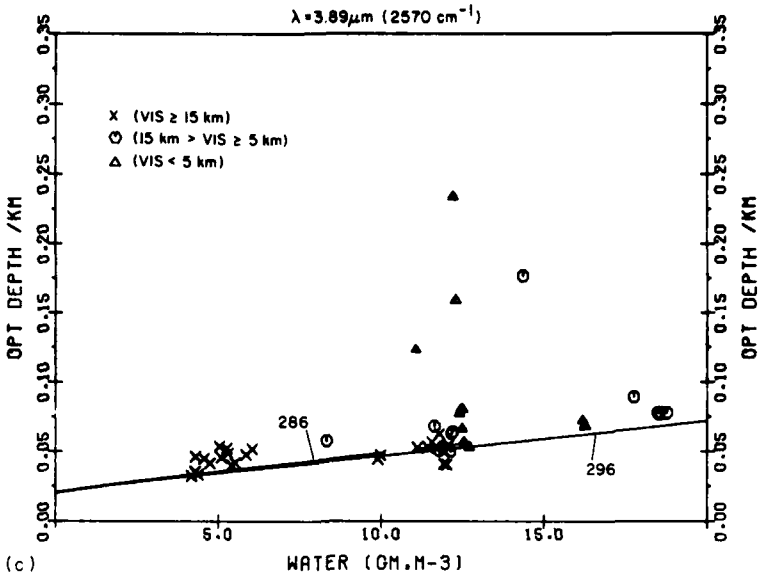

(c) 3.89-μm, Optical Depth/km Scale, All Data

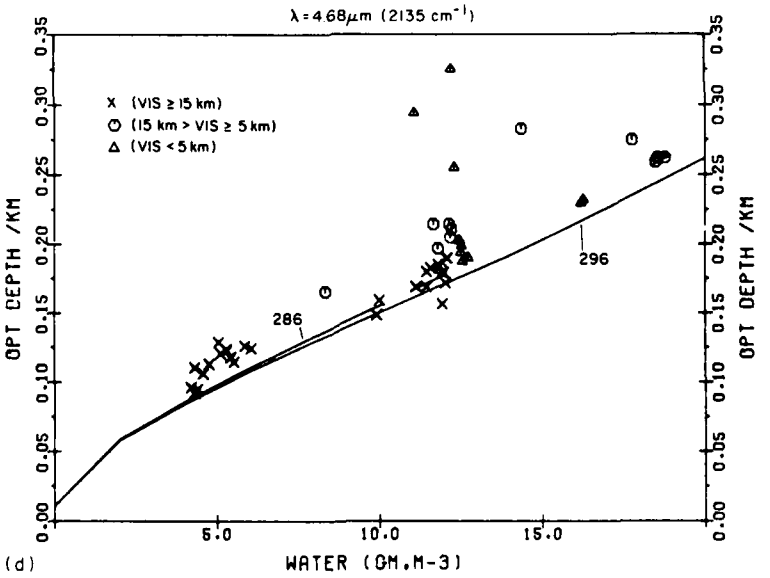

(d) 4.68-μm, Optical Depth/km Scale, All Data

Figure 19. Measured Transmittances (Symbols) and LOWTRAN Calculations (Solid Lines) at 286 and 296K for the 3- to 5-μm Region and the 8-km Path

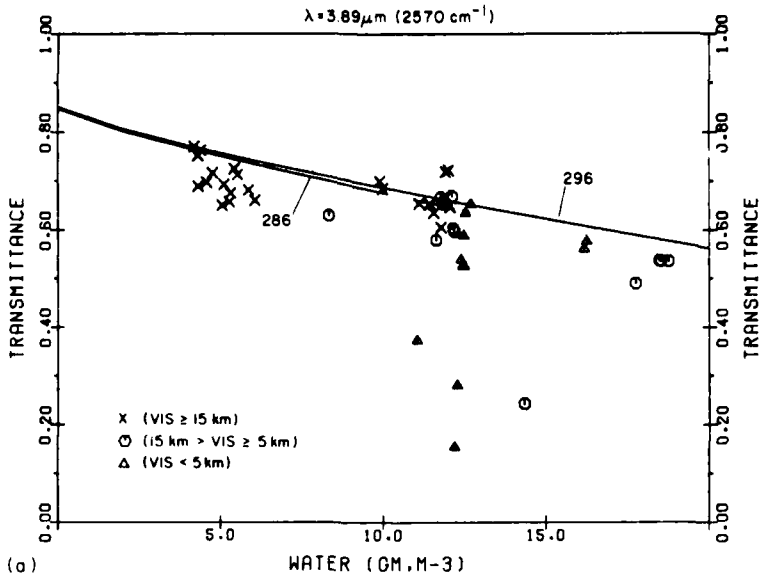

(a) 3.89-μm, Transmittance Scale, All Data

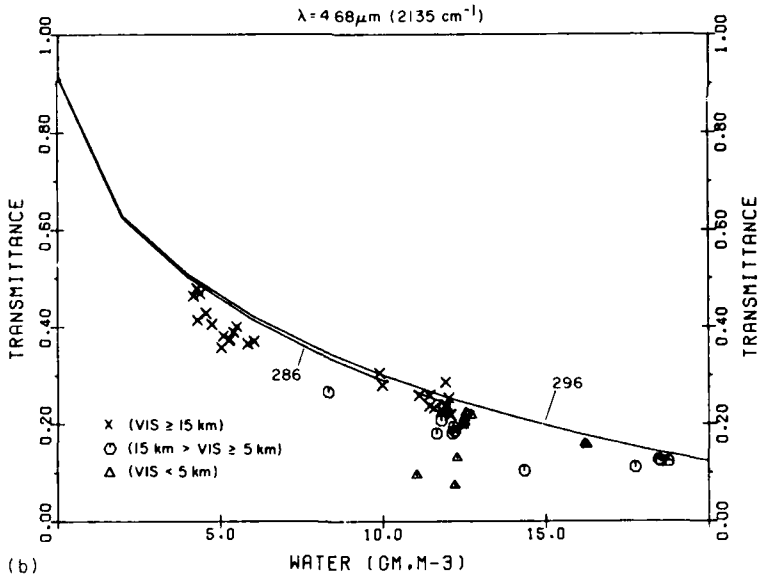

(b) 4.68-μm, Transmittance Scale, All Data

Figure 19. Measured Transmittances (Symbols) and LOWTRAN Calculations (Solid Lines) at 286 and 296K for the 3- to 5-μm Region and the 8-km Path

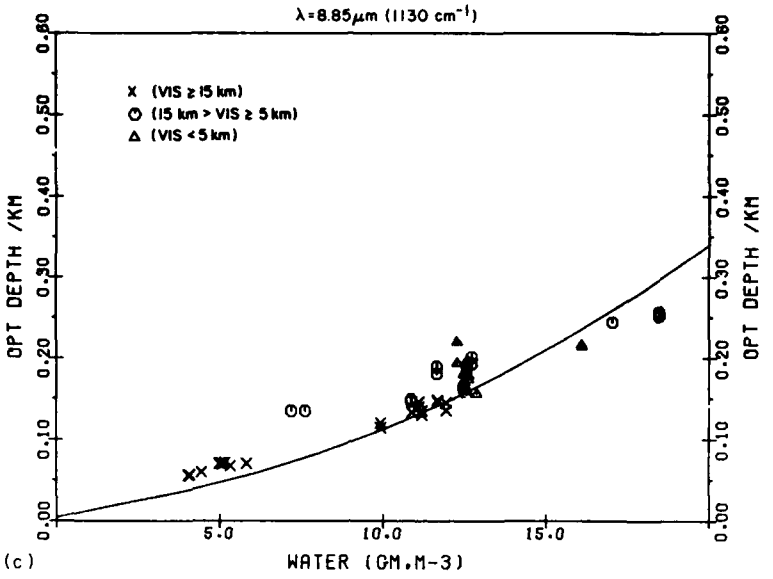

(c) 8.85-μm Filter, Optical Depth/km Scale, All Data

Figure 18. Measured Transmittances (Symbols) and LOWTRAN Calculation at 296K Degraded with a 6 percent CVF Filter, for the 8- to 12-μm Region and 8-km Path

small particles, which can cause a significant reduction in visibility but cause very little attenuation at infrared wavelengths. Verification of this theory requires the simultaneous measurement of atmospheric transmittance at visible and infrared wavelengths and detailed measurements of aerosol properties.

The 8- to 12-μm data for high water amounts along the 8-km path shows less extinction than LOWTRAN. One possible explanation is the breakdown of the pressure squared dependence of the water vapor continuum absorption. However, this conclusion would be contrary to the observations of other investigators (see Appendix C). Also, the number of data points involved is small, and the effect is not observed in the 2.25-km data.

More measurements are needed, preferably with humidity measurements taken at all three data poles, to determine if this effect is real.

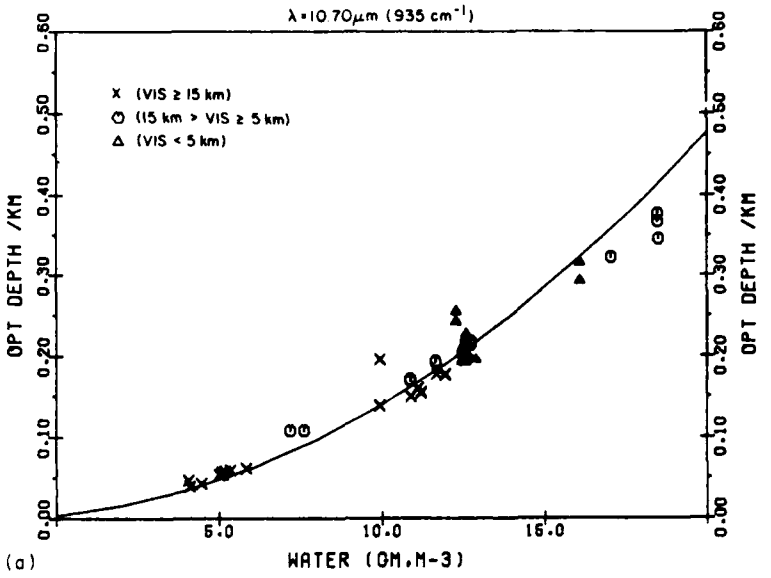

(a) 10.70-μm Filter, Optical Depth/km Scale, All Data

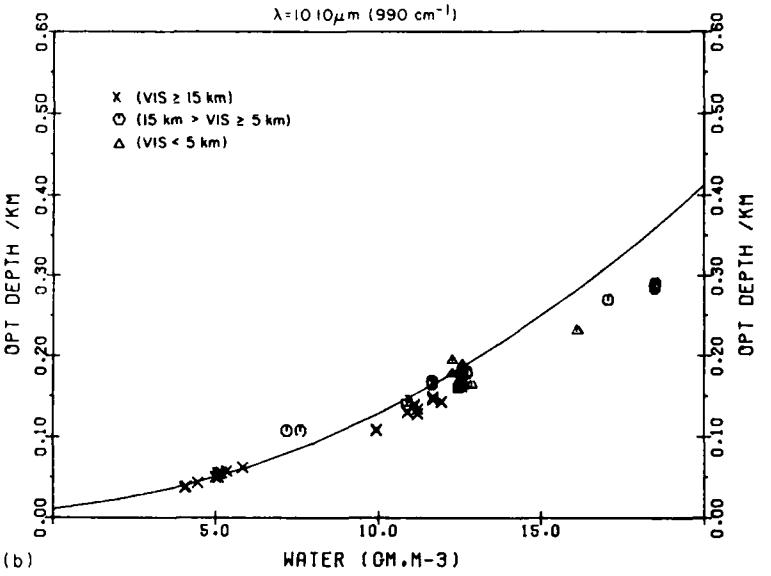

(b) 10.10-μm Filter, Optical Depth/km Scale, All Data

Figure 18. Measured Transmittances (Symbols) and LOWTRAN Calculation at 296K Degraded with a 6 percent CVF Filter, for the 8- to 12-μm Region and 8-km Path

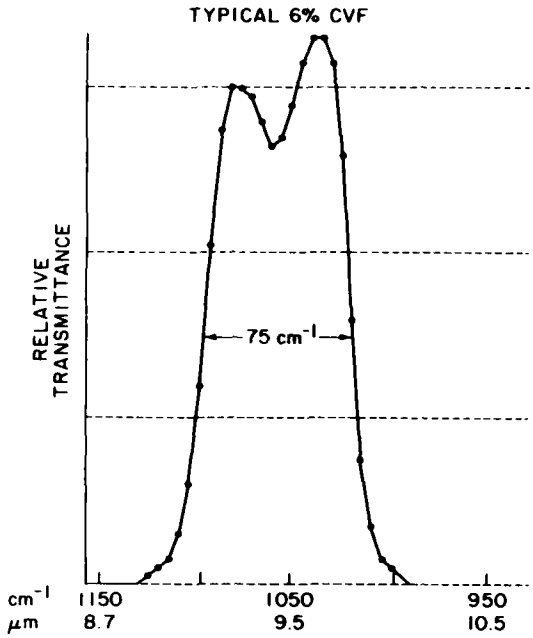

Figure 17. Relative Transmittance of a Typical 6 percent CVF Filter in the 10.0-μm Region

The effect of the 6 percent CVF on the LOWTRAN calculation is seen by comparing Figure 15 (d), (e), and (f) with Figure 18 (a), (b), and (c) (the data points in both cases are the same). For all three filters, the degraded calculations show slightly greater extinction. The maximum effect, however, is less than 8 percent of the optical depth per km, so that conclusions based on the undegraded LOWTRAN calculation are still valid.

The data for the 3- to 5-μm filters shown in Figures 19 and 20 exhibit behavior similar to the 8- to 12-μm data. The high visibility points agree reasonably well with LOWTRAN calculations as do many of the moderate and low visibility points. In particular, note the agreement for the 4.68-μm filter where previously LOWTRAN had no continuum coefficient and seriously underestimated the absorption. This data does, however, show greater scatter than the 8- to 12-μm data, with more points showing large discrepancies with LOWTRAN calculations.

3.5 Conclusions

The data shows generally good agreement between LOWTRAN calculated with no aerosols and the measurements made under conditions of low visibility. A possible explanation for this effect is that the aerosols are composed of very

Appendix B

Observer's Comments (Weather, Visibility, etc.)

7 May 81

Very clear. We could see open window of shack at Building 620 through telescope at Trebein. Visibility estimated > 60 km. Nephelometer readings* 0.03 to 0.06. Forward scatter meters not operational. The pressure readings on the attached weather summary are not valid. Called WPAFB weather station and their station pressure during the runs was 990 mb. Intensity scintillation was severe.

8 May 81

Clear, but not as clear as 7 May. Visibility estimated > 40 km. Nephelometer readings 0.08 to 0.10. Forward scatter meters not operational. The pressure readings on weather summary not valid. WPAFB weather station pressure was 989 mb. Intensity scintillation was severe.

11 May 81

Cloudy, foggy, with a fine mist of rain. The visibility was estimated at 2 through 4 km. Nephelometer readings were 0.15 to 0.18. No forward scatter meter. WPAFB weather station pressure was 981 mb. The signal stabilized at beginning of run but deteriorated at 3.98-μm position. The scan was continued and we repeated the 3.98-μm position about 8 min later under light rain conditions.

*Nephelometer units are km^{-1}.

No 8- to 14-μm runs were made because it began to rain very hard at conclusion of 3- to 5-μm run. The plots show the 3- to 5-μm measurements compared to LOWTRAN 5, with no aerosols, IHZ = 0, and with IHZ = 1, visibility = 8 km. Very little intensity scintillation.

12 May 81

Clear to very clear. The visibility was estimated at > 50 km. Nephelometer readings 0.05 to 0.07. Forward scatter meters not operational. WPAFB weather station pressure during runs was 983 mb. The plots show the 3- to 5- and 8- to 14-μm measurements compared to LOWTRAN 5 with no aerosols, IHZ = 0, and with IHZ = 1, visibility = 40 km. Intensity scintillation was severe.

19 May 81

Cloudy, with rain occurring in the early morning prior to runs. The visibility was estimated at > 20 km. Nephelometer readings 0.07 to 0.09. No forward scatter meter data. WPAFB weather station pressure during runs was 985 mb. All plots show the measurements compared to LOWTRAN 5 with no aerosols, IHZ = 0. The 1416Z, 3- to 5-μm plot also compares the measurements with IHZ = 1, visibility = 20 km. Intensity scintillation was very weak.

20 May 81

Sunny and bright. The visibility was estimated at > 30 km. Nephelometer readings 0.06 to 0.08. No forward scatter meter data. WPAFB weather station pressure during runs was 989 mb. Intensity scintillation was weak.

22 May 81

Sunny with haze and/or patchy ground fog. Visibility estimated > 8 km. Tower at Building 620 visible from Trebein. Nephelometer readings 0.23 to 0.27. WPAFB weather station pressure was 990 mb. Intensity scintillation was very strong.

27 May 81

Solid overcast, haze, some light drizzle, Building 620 barely visible from Trebein. Visibility estimated at 8 km. Only one run possible because of rain. Nephelometer readings 0.25 to 0.27. Forward scatter meters not operational. WPAFB weather station pressure was 979 mb. No intensity scintillation.

28 May 81

Very hazy, foggy with light drizzle or rain during early runs. Several observers estimated visibility at 2 to 4 km even after rain ended, no later than 1330Z. Nephelometer readings 0.3 to 0.5. No forward scatter meters. WPAFB weather station pressure was 979 mb at 1100Z and 982 mb at 2000Z. All plots show the measurements compared to LOWTRAN 5 with no aerosols, IHZ = 0. The 1356Z 8- to 14-μm measurements are also compared to LOWTRAN 5, IHZ = 1, IHZ = 8, and IHZ = 9 with visibilities of 4 and 8 km. No intensity scintillation.

2 June 81

Very hazy and foggy. Transmissometer operator could not see front gate at Trebein when he arrived. Could not get any signals until 1500Z. At this time he estimated visibility as 4 km at most. Nephelometer readings 0.28 to 0.35 at Pole 0. No forward scatter meter operational. WPAFB weather station pressure during run was 985 mb. No intensity scintillation.

11 June 81

Some haze. Visibility estimated > 10 km. Nephelometer readings 0.12 to 0.20. No forward scatter meter data. Pressure readings at Pole 0 on weather summary about 10 mb low. Low to moderate intensity scintillation.

12 June 81

Hazy, hot, and humid. Rain showers in area. 3- to 5- and 8- to 14-μm runs were probably effected by some drizzle or light rain. Visibility estimated > 10 km. Nephelometer readings 0.23 to 0.26. No forward scatter meter data. Pressure readings at Pole 0 on weather summary about 10 mb low. Low to moderate intensity scintillation.

15 June 81

Some haze, hot, and humid. Visibility estimated > 10 km. Nephelometer readings 0.14 to 0.17. No forward scatter meter data. Pressure readings at Pole 0 on weather summary about 10 mb low. Moderate scintillation.

17 June 81

Clear, but very light haze. Visibility estimated > 40 km. Nephelometer readings 0.05 to 0.08. No forward scatter meter data. Pressure readings at Pole 0 on weather summary about 10 mb low. High intensity scintillation.

19 June 81

Very heavy haze. Operator at receiver site said he could see Building 620 at times but estimated visibility as 7 to 8 km. Observer at mobile facility on runway observing area of downtown Dayton estimated visibility never got better than 12 km. Nephelometer readings 0.30 to 0.39. No forward scatter meter data. Pressure readings at Pole 0 about 10 mb low. Moderate to heavy intensity scintillation. Transmission data was compared to LOWTRAN 5 with IHZ = 0, no aerosols, and with IHZ = 1, visibilities of 8 and 12 km.

22 June 81

Very clear. Pressure readings at Pole 0 about 10 mb low. Moderate scintillation.

23 June 81

Very clear. Pressure readings at Pole 0 about 10 mb low. Moderate scintillation.

24 June 81

Very clear. Pressure readings at Pole 0 about 10 mb low. Moderate scintillation.

30 June 81 - No comments.

22 July 81

Some haze. Visibility estimated as > 10 km. Nephelometer readings 0.20 at Pole 0, 0.10 at the mobile. Pressure readings 10 mb too low.

23 July 81

Clear, visibility estimated as > 20 km. Nephelometer readings 0.08 to 0.10 at Pole 0. Pressure readings 10 mb too low.

24 July 81 - No comments.

27 July 81

Very foggy and hazy. Visibility estimated at 2 to 3 km. Pressure readings 10 mb too low. Could not see receiver van or Air Force Museum from source. Nephelometer readings 0.51 to 0.52.

29 July 81

Clear. Visibility estimated as > 20 km. Pressure readings 10 mb too low. Nephelometer readings 0.05 to 0.07.

4 Aug 81

Foggy and hazy. Visibility estimated as 7 km for early runs and 10 km for later runs. Pressure reading 10 mb too low. Nephelometer readings 0.34 to 0.37.

11 Aug 81

Some haze. Visibility estimated at 10 km. Pressure readings 10 mb too low. Nephelometer readings 0.14 to 0.18.

13 Aug 81

Some haze. Visibility estimated at 10 to 15 km. Pressure reading 10 mb too low. Nephelometer readings 0.19 to 0.20.

14 Aug 81

Considerable haze and fog. Visibility estimated at 3 to 5 km. No weather support due to computer shutdown. Temperature and dew point measurements taken with sling psychrometer.

17 Aug 81

Very clear. Visibility estimated at > 25 km. Pressure readings 1 mb too low. Nephelometer readings 0.05 to 0.06.

Appendix C

Water Vapor Continuum (LOWTRAN 6)

A new water vapor continuum model has been added to LOWTRAN 6.[C1] This model for the continuum contribution from water vapor absorption was originally developed by Clough et al[C2] for use with the line-by-line transmittance and radiance atmospheric code, FASCODE.[C3]

For atmospheric applications it is advantageous to express the density dependence of the water vapor continuum absorption in terms of a self and foreign component. The continuum contribution to the absorption coefficient $k_C(\nu)$, is given by the expression

$$k_C(\nu) = \rho_s \nu \tanh(hc\nu/2kT)\left[\left(\frac{\rho_s}{\rho_o}\right)\tilde{C}_s(\nu, T) + \left(\frac{\rho_f}{\rho_o}\right)\tilde{C}_f(\nu, T)\right] \quad , \qquad (C1)$$

where T is the temperature (°K), ν the wavenumber (cm^{-1}), $hc/k = 1.43879$ °K/cm^{-1} (ρ_s/ρ_o) and (ρ_f/ρ_o) are the number density ratios for the self and foreign continuum; and $\tilde{C}_s$ and $\tilde{C}_f$ [$(cm^{-1}\ mol/cm^2)^{-1}$] are wavenumber dependent continuum absorption parameters for the self and foreign components. The density ρ_s is the density of the water vapor and ρ_f is the density of all other molecular species; consequently, $\rho_s + \rho_f$ represents the total density. The quantity, ρ_o, is

---

The references cited above will not be listed here. See References, page 62.

the reference number density defined at 1013 mb and 296K. The present formulation in terms of density has the advantage that the continuum contribution to the absorption coefficient decreases with increasing temperature through the number density ratio term. The quantities $\tilde{C}_s$ and $\tilde{C}_f$ for water vapor are stored in the program for the spectral range 0 to 20,000 cm^{-1}.

The values for $\tilde{C}_s$ for water vapor at 296K are shown in Figure C1 together with the experimental values obtained by Burch et al.[C4-C7] The strong temperature dependence of the self density dependent water vapor continuum is treated by storing values of C_s at 260 and 296K and linearly interpolating between the 260 and 296K values. The 260K result was obtained by extrapolating the fits to the 338 and 296K data of Burch et al.[C6] The results for 260 and 296K are shown in Figure C2.

Only values near room temperature are available for the foreign dependence of the water vapor continuum. The continuum values $\tilde{C}_f$ at 296K are shown in Figure C3 and have been obtained by a fit to the data of Burch. There is still considerable uncertainty in the foreign values for the spectral window regions at 1000 and 2500 cm^{-1}.

In the LOWTRAN code, the total optical depth due to water vapor continuum absorption for an atmospheric slant path of N layers is given by

$$\sum_{i=1}^{N} \int_i k_c(\nu) ds = C_s(\nu, 296) \sum_{i=1}^{N} \int_i \left(\frac{\rho_s}{\rho_o}\right) \rho_s \, ds +$$

$$[C_s(\nu, 260) - C_s(\nu, 296)] \sum_{i=1}^{N} \left(\frac{296 - T_i}{296 - 260}\right) \int_i \left(\frac{\rho_s}{\rho_o}\right) \rho_s \, ds +$$

$$C_f(\nu, 296) \sum_{i=1}^{N} \int_i \left(\frac{\rho_f}{\rho_o}\right) \rho_s \, ds \quad , \tag{C2}$$

where ds is the incremental path length, T_i is the temperature of the i'th layer, and

$$C_s(\nu, 296) = \nu \tanh(hc\nu/2k(296))\, \tilde{C}_s(\nu, 296)$$
$$C_s(\nu, 260) = \nu \tanh(hc\nu/2k(260))\, \tilde{C}_s(\nu, 260)$$
$$C_f(\nu, 296) = \nu \tanh(hc\nu/2k(296))\, \tilde{C}_f(\nu, 296) \quad . \tag{C3}$$

The references cited above will not be listed here. See References, page 62.

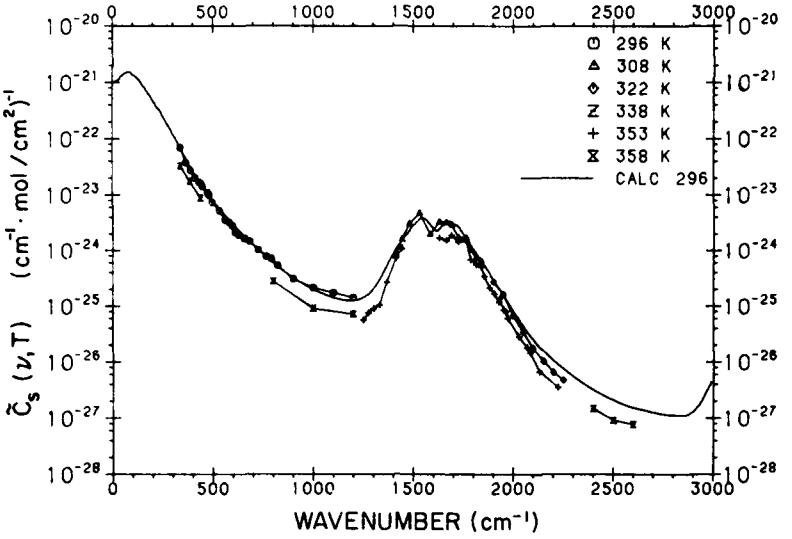

Figure C1. The Self Density Dependent Continuum Values, $\tilde{C}_s$, for Water Vapor as a Function of Wavenumber. The experimental values are from Burch et al[C4]

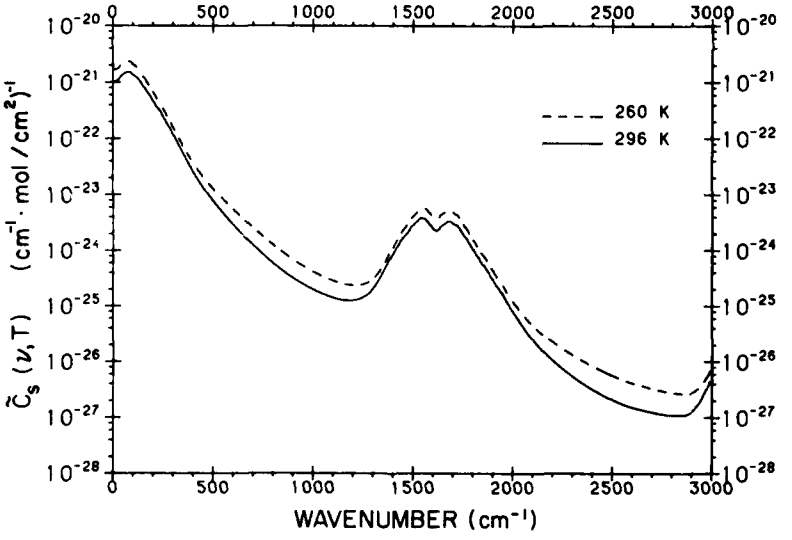

Figure C2. The Self Density Dependent Continuum Values, $\tilde{C}_s$, for Water Vapor as a Function of Wavenumber at 260K and 296K. The values from 296K are fits to experimental results; the 260K result is extrapolated

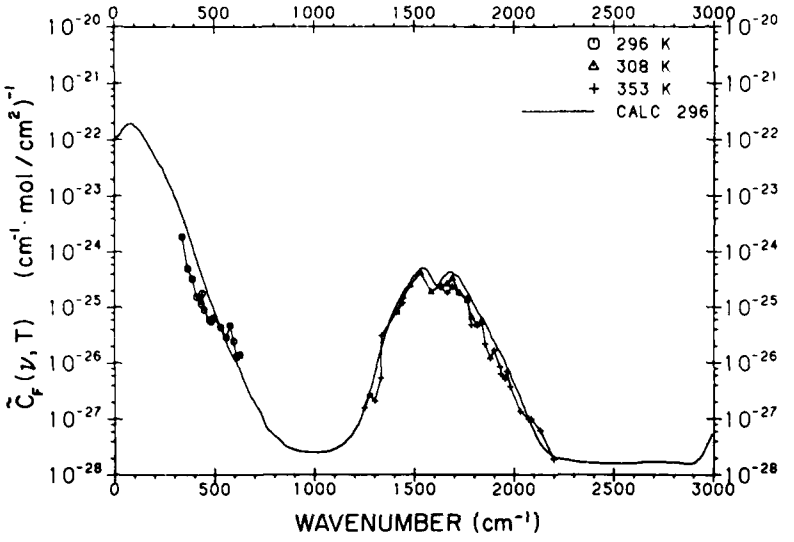

Figure C3. The Foreign Density Dependent Continuum Values, C_f, for Water Vapor as a Function of Wavenumber. The experimental values are from Burch et al[C4]

Calculations of atmospheric slant path transmittance using the new water vapor continuum absorption coefficients will result in approximately the same attenuation as in the LOWTRAN 5 model for the atmospheric window regions from 8 to 12-μm and 3.5 to 4.2-μm. However, for other spectral regions, particularly from 4.5 to 5.0-μm, significant improvement in atmospheric transmittance calculations has been made with the inclusion of the contribution of continuum absorption.

References

C1. Kneizys, F.X., Shettle, E.P., Gallery, W.O., Chetwynd, Jr., J.H., Abreu, L.W., Selby, J.E.A., Clough, S.A., and Fenn, R.W. (1983) Atmospheric Transmittance/Radiance: Computer Code LOWTRAN 6, AFGL-TR-83-0187, AD A137786.

C2. Clough, S.A., Kneizys, F.X., Davies, R., Gamache, R., and Tipping, R.H. (1980) Theoretical line shape for H_2O vapor; application to the continuum, Atmospheric Water Vapor, A. Deepak, T.D. Wilkerson, and L.H. Ruhnke, Eds., Academic Press, New York.

C3. Clough, S.A., Kneizys, F.X., Rothman, L.S., and Gallery, W.O. (1981) Atmospheric spectral transmittance and radiance: FASCODE 1B, Proc. of SPIE, The Inter. Soc. for Opt. Eng., 277, Atmospheric Transmission, R.W. Fenn, Ed.

C4. Burch, D.E., and Gryvnak, D.A. (1979) Method of Calculating H_2O Transmission Between 333 and 633 cm^{-1}, AFGL-TR-79-0054, AD A072850.

C5. Burch, D.E., and Gryvnak, D.A. (1978) Infrared Absorption by CO_2 and H_2O, AFGL-TR-78-0154, AD A060079.

C6. Burch, D.E., Gryvnak, D.A., and Pembroke, J.D. (1971) Investigation of Absorption by Atmospheric Gases, AFCRL-71-0124, AD A882876.

C7. Burch, D.E. (1970) Semi-Annual Technical Report, Aeronutronic Report No. U-4784.

END

FILMED

6-85

DTIC